CONTRIBUTED PAPER

Radio Frequency Switches Based on Emerging Resistive Memory Technologies: A Survey

This article surveys high-performance radio frequency (RF) switches based on resistive memories, comparing them to mature RF switching technologies, and discusses future prospects and research directions for this technology.

By Nicolás Wainstein, *Graduate Student Member IEEE*, Gina Adam, *Member IEEE*, Eilam Yalon, *Member IEEE*, and Shahar Kvatinsky, *Senior Member IEEE*

ABSTRACT | High-performance radio frequency (RF) switches play a critical role in allowing radio transceivers to provide access to shared resources such as antennas. They are important, especially in reconfigurable radios, where the connections within and between the different blocks (e.g., filters, amplifiers, and mixers) can be changed to customize and compose RF functions for distinct frequency bands. To realize this potential, new concepts for RF switch devices that can be integrated with standard transistor process, while providing better transmission performance, lower power consumption, smaller area, and lower actuation voltage than current RF switch technologies [e.g., field-effect transistors (FETs) and microelectromechanical systems (MEMSs)] are needed. Recently, RF switches based on emerging memory technologies, such as conductive-bridge RAM (CBRAM), resistive RAM (ReRAM), and phase-change memory (PCM), have been proposed. These nanoscale switches present major advantages, for example, high cutoff frequency, nonvolatility, fast and low-energy switching, small footprint, and compatibility with back-end-of-line (BEOL) of the standard CMOS process, thus placing them as possible contenders for high-performance RF switches. This article surveys high-performance RF switches based on resistive memories, comparing them with mature RF switching technologies like RF MEMS, p-i-n diodes, and FETs. We discuss the physical mechanisms, device structure, performance characteristics, and applications of these novel RF switches. Furthermore, we examine the prospects and future research directions of these technologies that could lead to their adoption at the industrial level.

KEYWORDS | Conductive-bridge RAM (CBRAM); emerging memory; inductors; monolithic wireless transceivers; multiband; phase-change memory (PCM); p-i-n diode; radio frequency (RF); reconfigurable radios; resistive memory; resistive RAM (ReRAM); RF microelectromechanical systems (MEMSs); RF integrated circuits (RFIC); RF switches; switches; tunable circuits; wireless communications.

Manuscript received April 8, 2020; revised June 19, 2020; accepted July 22, 2020. Date of publication August 7, 2020; date of current version December 21, 2020. This work was supported in part by the Israel Innovation Authority KAMIN under Grant 66769, in part by the European Commission under Grant MSCA-IF-705957, and in part by the Russell Berrie Nanotechnology Institute (RBNI). *(Corresponding author: Nicolás Wainstein.)*

Nicolás Wainstein, **Eilam Yalon**, and **Shahar Kvatinsky** are with the Andrew and Erna Viterbi Faculty of Electrical Engineering, Technion–Israel Institute of Technology, Haifa 32000, Israel (e-mail: nicolasw@campus.technion.ac.il; eyalon@ee.technion.ac.il; shahar@ee.technion.ac.il).

Gina Adam is with the Department of Electrical and Computer Engineering, The George Washington University, Washington, DC 20052 USA (e-mail: ginaadam@gwu.edu).

Digital Object Identifier 10.1109/JPROC.2020.3011953

I. INTRODUCTION

It has been predicted that by 2020 there will be more than 50 billion mobile communication devices [1], further increasing the heterogeneity of radio frequency (RF) standards in the wireless communication ecosystem (see Fig. 1). At the same time, there is a growing market demand for multiband cellphones and wearable devices that are spectrally efficient and can be used across the world. Currently, multiband radio transceivers comprise

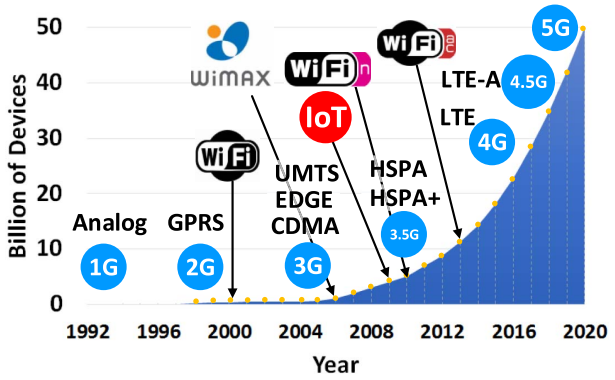

Fig. 1. *Mobile communication trends. Growth of mobile-connected devices over the last three decades. Inset: the mobile communication standards implemented during those years. Data taken from [1].*

multiple high-frequency RF chains for each band, including filters, amplifiers, and mixers [2], [3]. For instance, a six-band radio transceiver will have six RF paths and state-of-the-art smartphones such as the iPhone X support approximately 25 of the 66 LTE available bands [4]. Moreover, the requirement for backward compatibility requires support of global system for mobile communications (GSM) and 3G standards. Clearly, this solution is not scalable without improved integration and miniaturization. The question is how to maintain the miniaturization trend, low power consumption, and high performance as the number of standards continues to increase. The answer is through reconfigurable radios that can support multiple frequency bands, and the coexistence of several wireless communication standards (i.e., multistandard).

Software-defined radios (SDRs) are the digital approach for reconfigurable RF systems. In these systems, many components of the radio transceiver that are usually implemented by hardware (e.g., filters, mixers, amplifiers, modulators) are implemented by software and performed on a digital signal processor (DSP). Thus, the DSP must process a huge amount of data, at high speeds (i.e., sampling rate) and with high resolution, leading to a huge power consumption, prohibitive for a portable device [5], [6]. Another concern is whether the radio sensitivity of SDRs can be as high as that of a cellphone device since they require wide bandwidth components.

An alternative approach is to use reconfigurable hardware RF architectures, whose components can be tuned among widely distributed frequency bands. In such architectures, the analog-to-digital converters (ADCs), mixers, filters, and amplifiers can be adjusted by reconfiguring them or by changing the connection differently, to adjust the receiver and transmitter chains, thus reducing (or even eliminating) the need for a separate RF chain for each band. Blocks can be thus reutilized and redundant components eliminated, enabling greater flexibility and radically reducing the form factor and the complexity of wireless front-ends. This in turn reduces system costs and development time. Among the technologies that can enable hardware-reconfigurable multistandard radios are all-digital receivers, digital phase-locked loop (PLL), tunable filters, and high-performance RF switches [7]. Certainly, a mixed approach between software-defined and hardware reconfiguration could be used, considering the tradeoffs between flexibility, power budget, area, cost-effectiveness, and performance.

In a reconfigurable architecture, the RF switch is a fundamental component for controlling the flow of the RF signal and providing tunable capabilities to filters, amplifiers, and other components [8]. Solid-state and microelectromechanical systems (MEMSs) are the most common integrated technologies for RF switches. MEMSs are superior to compound and silicon-based field-effect transistor (FET) switches in terms of energy consumption and RF transmission parameters. However, they suffer from several performance and reliability issues such as dielectric charging, low switching speed, contact interface degradation, and large area overhead [9]. FET-based switches provide fast switching but require a relatively large area to achieve a low resistance in the ON-state, which results in a large parasitic capacitance [10], [11]. p-i-n diodes can achieve excellent transmission performance, but they require a bias current to maintain the ON-state. Hence, the search continues for RF switches that can be easily integrated, have high transmission performance, low power consumption, and high power handling.

Recently, resistive memory technologies, such as resistive RAM (RRAM or ReRAM), conductive-bridge RAM (CBRAM), and phase-change memory (PCM), have emerged as promising candidates for high-performance RF switches [12]–[14], thanks to their superb transmission properties, small footprint, short switching time, low-energy consumption, scalability, and nonvolatility. Furthermore, these devices can be fabricated in the back-end-of-line (BEOL) of standard CMOS process, which can reduce the need for routing signals from the top metal layer to the transistor layer, hence reducing the power losses and inherent area overhead. Therefore, these technologies can also add tunability to passive devices that traditionally stand on the top metal layers (e.g., metal–insulator–metal (MIM) capacitors, and spiral inductors), providing the required reconfigurability to face the new challenges in communications.

In this article, we present a focused survey of the different resistive memory-based RF switches and their applications in front-end RF systems. In Section II, we present the switching dynamics, materials, and key performance metrics of resistive memory technologies. In Section III, we survey the high-performance RF switch technologies and their critical performance parameters. We present the device characteristics and performance of resistive memory-based RF switches in Section IV, and their application in front-end circuits in Section V. Finally, Section VI concludes this article and discusses the prospects of ReRAM, CBRAM, and PCM-based RF switches in reconfigurable RF systems.

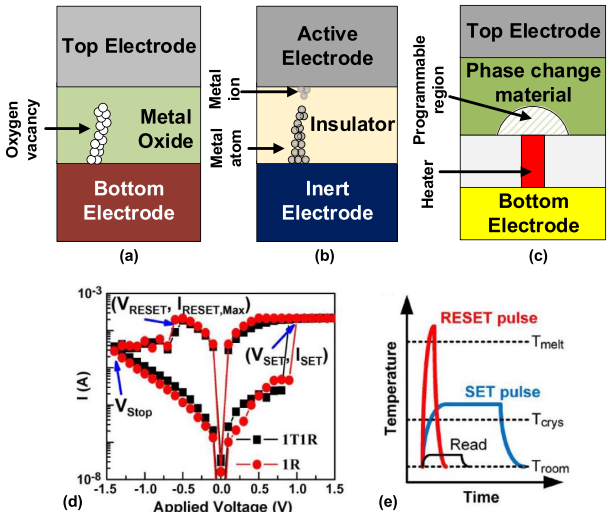

Fig. 2. *Structure of (a) ReRAM, (b) CBRAM, and (c) PCM devices. In ReRAM, the switching occurs in the metal-oxide layer, while in CBRAM the switching is ruled by the movement of metal ions from the active electrode. In PCM, the switching occurs in the programmable region as a phase change between crystalline and amorphous in chalcogenide. (d) Typical I–V curve of ReRAM and CBRAM devices (taken from [27]). (e) Typical PCM programming pulses (taken from [19]).*

II. RESISTIVE MEMORY TECHNOLOGIES

Nonvolatile resistive memories are a group of emerging memory technologies that store information as different resistive states. They are typically two-terminal (though three- and four-terminal devices exist) passive devices with varying resistance, where the resistive state can be electrically controlled. This heterogeneous conglomerate of devices includes ReRAM, CBRAM, PCM, and magnetoresistive RAM (MRAM). The physical actuation varies among the different technologies, but they are usually controlled by electrical field, current, and/or heat (as in PCM).

These devices can be used as switches with discrete states, as they exhibit nonlinear switching behavior associated with electric field and/or temperature-accelerated atom or ion movement [15]. The time required to switch the devices varies dramatically (exponentially or even superexponentially) with the applied voltage. The high resistive state (HRS, R_{OFF}) is achieved after a "reset" programming and the low resistive state (LRS, R_{ON}) is achieved after a "set" operation [see Fig. 2(e)]. Furthermore, some devices exhibit intermediate resistive levels [15], which allows for their use as multilevel cells in memory arrays [16] and as artificial synapses in neuromorphic applications [17], [18]. For RF switching applications, their use is focused on the binary states (R_{ON}, R_{OFF}). Their nonvolatility implies that no bias voltage or current is required to maintain a particular state, eliminating the static power consumption, and hence potentially reducing the overall energy consumption. Furthermore, they can potentially achieve high endurance, exhibit fast switching, low switching energy, and have a small footprint [19]–[21].

Since BEOL compatibility is crucial for integration of these devices with CMOS technology, extensive work has been done to identify not only devices that perform well, but can also be fabricated via low-temperature processes and with materials compatible with CMOS. Moreover, these can be stacked in a 3-D fashion in a crossbar architecture with a memory cell area of $4F^2/n$, where F is the feature size of the technology and n is the number of stacked layers [20], [22], [23]. These characteristics make them promising candidates for memory [19], [20], [23], [24], logic within memory [25], and neuromorphic computing [26].

A. Resistive RAM

ReRAM or valence-change memory (VCM) consists of a metal oxide sandwiched between two metal electrodes in an MIM structure [20] [see Fig. 2(a)]. Upon external stimuli, oxygen anions are prone to move in the oxide lattice, leaving "oxygen vacancies," which cause changes in the oxide resistance [28]. Virgin devices typically require an electroforming process [20], which requires higher voltages than the set voltage, to prompt the future resistive switching process. After electroforming, a conductive filament is formed and the LRS is achieved. Subsequent set–reset cycles will only partially change this filament. The reset process is governed basically by Joule heating and ion migration. Oxygen ions migrate back to the oxygen vacancies or oxidize the conductive filament increasing the resistance to HRS.

Another subcategory of ReRAM is the binary nonfilamentary metal-oxide memory. Its uniqueness relies in that it is completely based on an interfacial effect. Hence, the OFF- and ON-currents depend linearly on the device area and not on a metallic filament, and thus there is no need for an electroforming step [29], [30]. The device consists of a conductive metal oxide with a thin insulating metal oxide tunneling layer sandwiched between two inert electrodes. The switch relies on changes on the potential barrier owing to field-dependent oxygen exchange between the two layers [29], [30].

A broad variety of oxides have been proposed for these devices, for example, hafnium oxide (HfO_x), tantalum oxide (TaO_x), and titanium oxide (TiO_x), and many metals have been proposed for the electrodes, such as titanium (Ti), titanium nitride (TiN), platinum (Pt), and aluminum (Al) [22]. Particularly, HfO_2 is already being used as a high-k dielectric in several CMOS processes. Therefore, devices that use HfO_2 can readily be integrated with standard CMOS processes [20].

The very many possible combinations of electrode materials and metal oxides result in a wide variety of devices, differing in performance in terms of R_{OFF}–R_{ON} ratio, endurance, switching time, switching energy, and switching mode (unipolar or bipolar). The switching direction in unipolar devices depends on the amplitude of

the applied voltage/current regardless of the polarity. On the contrary, bipolar devices require voltage/current of opposite polarity to set/reset. The switching time in ReRAM devices has been shown to be in the order of nanoseconds, though subnanosecond switching has also been observed [31], [32]. Furthermore, ReRAM devices can achieve low power–energy consumption, with low set–reset currents (<100 nA), high endurance ($>10^{12}$ cycles) [33]–[35], and data retention >10 years [20]. ReRAM presents some reliability issues such as anomalous reset called negative set, where large currents are obtained after a reset operation owing to defect generation and injection from the bottom electrode (BE), which is positively biased during reset [36]. ReRAM can also present cycle-to-cycle resistance variation because of the stochastic number and position of defects in the filament and in the depleted gap. Furthermore, data retention is strongly dependent on the size of the conductive filament and the electroforming voltage [36]. The LRS resistance increases with time due to a gradual dissolution of the conductive filament. This phenomenon is accelerated in higher temperatures.

B. Conductive-Bridge RAM

CBRAM, also known as electrochemical metallization (ECM) memory, consists of a pair of electrochemically asymmetric metal electrodes (i.e., an active electrode and an inert electrode) separated by a small-scale gap or an insulator [21] as shown in Fig. 2(b). The switching mechanism relies on a redox process where a metallic filament is formed or ruptured between the two electrodes due to electrochemical reactions, ion migration, and Joule heating [24]. Hence, when an external electric field is applied between the electrodes, ions from the active electrode migrate to the inert electrode building up the filament. A field with opposite polarity reverses the process, that is, some of the metal ions from the filament dissolve and migrate back toward the active electrode, recombining with the bulk metal.

The active electrode can be silver (Ag), copper (Cu), or nickel (Ni), with Ag being the most popular. The inert electrode can be platinum (Pt), tungsten (W), or gold (Au), among others. As for the insulating material, it serves as a solid electrolyte; amorphous chalcogenides (compounds including Ge, S, Se, and Te) and oxides have been explored for this purpose [21]. For CMOS integration, diffusion barriers are required to prevent Ag or Cu contamination of the underlying transistors. Conversely, W is used for the inert electrode because it is prevalent in CMOS interconnects. For instance, in [37] SiO_2-based CBRAM devices are reviewed. Particularly, Cu-SiO_2-W CBRAM devices show promising performance and are fully compatible with current CMOS BEOL process.

An interesting property of these devices is the linear dependence of R_{ON} on the compliance current [13], [21]; the higher the compliance current, the lower the achieved R_{ON}. It has been demonstrated [38], [39] that this technology can achieve fast switching time (<10 ns), good endurance ($>10^6$), low power switching (<nW), scalability to sub-20 nm, good retention (>10 years), and high R_{OFF}/R_{ON} ratio ($>10^6$). Reliability issues in CBRAM include electrode oxidation and filament instability since the filament formation is intrinsically a stochastic process. Therefore, the LRS is prone to exhibit cycle-to-cycle variations. Furthermore, filament overgrowth can result in negative-SET behavior, which can result in reset failure [36]. These issues can be solved with process enhancements as shown in [40]. Also in CBRAM, the LRS is reported to increase with time and high temperatures [21]. It has been shown that lower LRS improves the retention, possibly due to thicker filaments.

C. Phase-Change Memory

PCM relies on the large ratio between the high resistance of the amorphous phase and the low resistance of the crystalline phase in phase-change materials [19]. Typical phase-change materials are chalcogenide compounds such as $Ge_2Sb_2Te_5$ (GST). Fig. 2(c) shows a typical "mushroom-type" cell, which consists of a phase-change material placed between two electrodes and heated from below by a refractory metal (heater). To reset the PCM, the lattice of the programming region must be rearranged in an amorphous manner (i.e., amorphization). Thus, the local temperature of the GST must rise above the melting temperature T_{melt} (typically above 600 °C), melting part of the phase-change material (i.e., programmable region), and must quickly be quenched to low temperature (below the crystallization temperature $T_{crys} \sim 200$ °C) so that the material does not have time to recrystallize. To achieve this temperature change, a large amplitude, short width pulse is applied [see Fig. 2(e)]. On the contrary, to crystallize (i.e., set) the cell, a small amplitude, long width pulse is applied. With this stimulus, the temperature of the phase-change material rises beyond T_{crys} allowing the lattice to recrystallize [41]. Thus, PCMs are unipolar since the switching dynamics do not depend on the polarity of the pulses.

PCM stands as a viable candidate for storage-class memory because of its inherent CMOS friendliness of the PCM cell materials [15], [23]. Stoichiometric variations of the GST achieve different R_{OFF}/R_{ON} ratio, endurance, set time and energy, reset time and energy, and retention. For instance, in [42], a device with 80-ns set time, endurance of over 10^9 cycles, and retention time of ten years was demonstrated. Although the crystalline state is almost constant, PCMs present state drift in the amorphous phase [15], [19]. The origin of the resistance drift is still debated, but it is a serious concern in multilevel cells and for their use as artificial synapses. Certainly, when using the PCM as an RF switch, the variability of the HRS is irrelevant since the OFF-state performance is further related to the OFF-state parasitic capacitance than R_{OFF}.

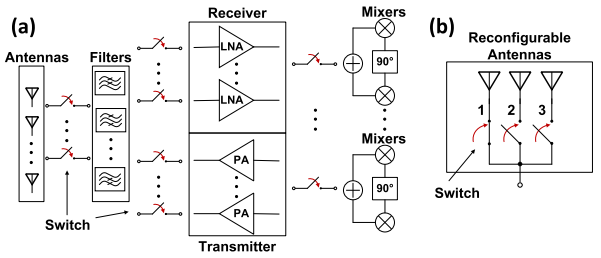

Fig. 3. *(a) Intercircuit reconfiguration. The connection between the different front-end blocks can be changed using high-performance RF switches. (b) Example of intracircuit reconfiguration in tunable antennas. The switch is used to select a subantenna or conversely, to change some parameter of the antenna (e.g., the resonance frequency).*

III. RF SWITCHES

RF switches are fundamental components in radio transceivers for the control of signal flow and to multiplex the access to shared resources or blocks (e.g., antennas, amplifiers, and filters). Particularly in reconfigurable systems, the RF switch provides tunability by changing the connection between different circuit blocks (i.e., intercircuit connections), as shown in Fig. 3(a), and within functional blocks (i.e., intracircuit connections) by changing the characteristics of the circuit block, as shown in Fig. 3(b). As depicted in Fig. 4, the basic model of an RF switch consists of a parallel *RC* circuit, with a varying resistance and a parasitic capacitor. The insertion loss (IL) (i.e., the signal loss in the ON-state) is determined by the ON-resistance (R_{ON}) of the switch, while the isolation (i.e., the undesired signal leakage in the OFF-state) is determined by the parasitic capacitance (C_{OFF}). The figure of merit (FOM) of RF switches is the cutoff frequency, at which the OFF-impedance equals the ON-impedance. Assuming the basic *RC* model, the cutoff frequency is $f_{\mathrm{CO}} = (2\pi R_{\mathrm{ON}} C_{\mathrm{OFF}})^{-1}$. Therefore, this FOM accounts for the main contributors to the IL and isolation.

Other critical metrics of the RF switch are bandwidth, return loss, maximum power handling, linearity, video leakage, crosstalk, switching time and switching energy, endurance, and footprint [43]. Power handling is determined as the maximum power that can be sustained by the RF switch during regular operation. Linearity is characterized by the third-order intercept (IP3), that is, the power at which the third harmonic equals that of the fundamental, and the 1-dB compression point ($P_{1\ \mathrm{dB}}$), that is, the input power at which the output power decreases 1 dB from the input power.

RF switches can be categorized in two main groups: solid-state and electromechanical. The former group includes devices based on controlled electron flow through semiconductors. The latter includes devices that rely on mechanical movement of a relay or a cantilever, usually controlled by voltage or current, to connect/disconnect an ohmic or capacitive contact. In this section, we discuss the main characteristics of solid-state (e.g., p-i-n diodes, CMOS, compound FETs) and MEMS RF switches.

A. Solid-State RF Switches

FET, p-i-n diodes, and hybrid diodes (FET and p-i-n) are the main solid-state switches. They are more reliable, exhibit higher endurance, have longer wear-out, and faster switching than the electromechanical switches since they operate without moving parts. However, they exhibit a higher ON-resistance, which results in higher signal power loss, that is, IL. Compound semiconductor switches from group III–V, such as gallium arsenide (GaAs), indium phosphide (InP), and aluminum arsenide (AlAs), have shown better performance than the Si-based switches because of higher electron mobility in these materials [44], particularly in indium-gallium-arsenide (InGaAs)-based high-electron-mobility transistors (HEMTs). However, III–V compounds have their own, that is, special fabrication process; thus, they require heterogeneous CMOS integration, which is still expensive and inefficient.

The p-i-n diode consists of an intrinsic (I) layer, sandwiched between a p-type region (P) and an n-type region (N). The diode serves as a current-controlled variable resistor, with an ON-resistance lower than 1 Ω and OFF-resistance greater than 10 kΩ. These devices have high switching speed and small footprint. However, the bias current required to maintain the ON-state results in high power consumption. On the contrary, FET switches are controlled by the voltage applied between the gate and the source. Since they are four-terminal devices, there is an inherent isolation between the dc and RF paths. Furthermore, they are the preferred option in applications that require high endurance, reliability, and low switching time. The ON-resistance is inversely proportional to the width of the transistor. Therefore, to achieve a low resistance, the transistor width should be large enough ($>100\ \mu$m) [45]. On the contrary, the parasitic (drain-to-source) capacitance is directly proportional to the transistor width. Hence, FET switches achieve low IL at the expense of a poor IS, and their FOM is lower than that of the p-i-n diode. Due to their low IS, most applications require two FET switches to fulfill the minimum IS requirements.

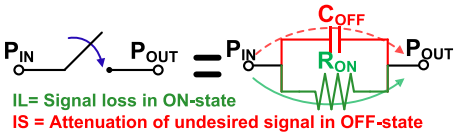

Fig. 4. *First-order model of an RF switch. The ON-resistance, R_{ON}, determines the IL (i.e., the signal loss in the ON-state). The OFF-capacitance, C_{OFF}, is the parasitic capacitance which determines the isolation, namely the attenuation level of unwanted signal flow.*

Table 1 Comparison Between High-Performance RF Switch Technologies

Parameter	RF MEMS	PIN	FET	MIT	ReRAM	CBRAM	PCM
Voltage	20–80 V	1–5 V	1–5 V	3-30 V	1–3 V	1–3 V	1–10 V
Switching Energy	50 pJ–10 μJ	50 fJ–10 nJ	50 fJ–10 pJ	0.1 nJ-40 μ W	0.01–1 nJ	1–100 nJ	1–500 nJ
Static Power Consumption	$\sim$0 mW[1]	5–100 mW	0.05–0.1 mW	$>$ 150 mW	0 W	0 W	0 W
Switching time	1–300 μs	1–100 ns	1–100 ns	2 ns–40 μs	1–100 ns	1–100 ns	100/1000 ns
FOM	20–50 THz	1–4 THz	0.5–2 THz	0.5–10 THz	$\sim$3 THz	3–70 THz	1–57 THz
Power handling	$<$ 0.5 W	$<$ 10 W	$<$ 10 W	$<$ 2 W	$<$ 1 W	$<$ 1 W	$<$ 10 W
Area (μm^2)	10^2–10^4	50–10^3	10–10^3	10^3-10^6	$\sim$1	$\sim$1	1-10^3
Maturity	****	*****	*****	***	*	**	***
# of Terminals	3	2	4	2/4	2	2	2-4

[1] Includes voltage upconverter and driving circuitry to maintain the state.

Vanadium dioxide (VO_2) is a phase-change material that presents metal-to-insulator transition (MIT) [46], [47]. This abrupt and reversible MIT occurs at a critical temperature. Contrary to other phase-change materials, the VO_2 MIT is volatile, that is, the temperature of the material must be above the critical temperature (68 °C) to maintain the conducting state, while at room temperature the material behaves as an insulator. Due to the high contrast between the insulating and metallic phases ($\sim 10^3$) and the low resistivity in the metal phase ($\rho < 12\ \mu\Omega \cdot$ m), VO_2 stands as an interesting material for RF switches [48]–[50]. Single-pole single-throw (SPST) devices based on VO_2 have shown an IL below 0.4 dB and IS better than 30 dB up to 20 GHz [51]. The switching time can be as low as $\sim$15 ns [49]. However, the dc ON-voltages can be larger than 3 V, with currents above 50 mA, thus incurring large static power consumption. In terms of area, these devices can be as small as $20 \times 20\ \mu$m^2. MIT RF switches have been used, among others, to implement broadband phase shifters [52] and power limiters [53]. An extensive review of RF switches and circuits based on MIT is presented in [47].

B. MEMS RF Switches

MEMS switches are surface-micromachined devices that can switch a transmission line based on the mechanical movement of one (or more) movable parts [57]. The RF MEMS switch consists of two parts: mechanical, for actuation, and electrical for control. The MEMS switch can be classified by the source of the physical phenomenon that controls the mechanical movement, which can be thermal, electrostatic, magnetostatic, and piezoelectric. Furthermore, they can be classified by the device orientation: vertical or horizontal, and according to the contact type in capacitive or metal-to-metal (ohmic). In capacitive contact switches, the transmission is changed owing to a large capacitance ratio ($>$500) between the OFF- and ON-states [58]–[61]. Electrostatic actuation is the most popular and attractive method because of the low energy consumption (10–100 nJ) per cycle. Developments in the past decade have made this technology an extremely attractive option as an RF switch, since these RF MEMS switches can achieve extremely low IL ($<$0.1–0.2 dB), low R_{ON} (0.5–2 Ω for metal-contact devices, 0.1–0.2 Ω for capacitive devices), low C_{OFF} (2–16 fF), very high isolation, and high linearity up to mm-wave frequencies [58]. However, most implementations of these devices require high actuation voltages of 30–80 V [9]. Commercial MEMS switches with 3-V operating voltages are nowadays available [62], where the MEMS switch is actuated by a charge pump that creates the 80 V required to switch the device. Furthermore, capacitive contact RF MEMSs are usually used as shunt switches, which results in poor isolation at low frequencies. Other drawbacks of these devices include low switching speeds (2–40 μs), low power handling ($\sim$23 dBm), reliability issues due to contact degradation and dielectric charging, costly or incompatible integration with CMOS, costly packaging, and high fabrication costs [57]. RF MEMS switches find application in several subsystems, for example, reconfigurable antennas [63], [64], and tunable filters [58], [65]. A summary comparison between the different RF switch technologies is listed in Table 1.

IV. HIGH-PERFORMANCE RESISTIVE MEMORY-BASED RF SWITCHES

Resistive memory-based RF switches have emerged as high-performance RF switches because of their state-of-the-art FOM, low switching energy, nonvolatility, and small area. Since their switching mechanism is an actual change in the physical structure of the devices (without moving mechanical parts), they could achieve better endurance than MEMS. Endurance remains a critical issue that requires further research and investment in terms of material research and processing to move from a research-grade device to industry-grade, reliable technology. Their nonvolatility results in a lower energy consumption, as no bias power is required to maintain the state as in FETs and p-i-n diodes. Furthermore, they achieve a state-of-the-art FOM requiring a much smaller area than their contenders. A survey of the FOM achieved in published

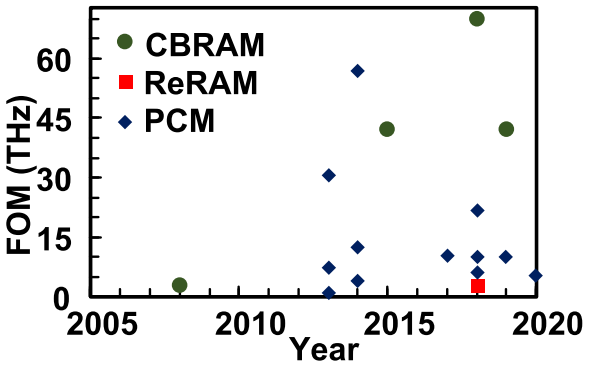

Fig. 5. *Survey of the FOM of published RF switches based on resistive memories.*

works since 2008 is presented in Fig. 5. The difference between these devices and their siblings for memory and logic is in their low ON-resistance (<10 Ω), and their small parasitic or OFF-capacitance (<15 fF). In these devices, the requirements for the R_{OFF}/R_{ON} ratio can be relaxed since an R_{OFF} greater than 10 kΩ is sufficient to achieve a decent isolation at low frequencies. To achieve dc decoupling, three- and four-terminal devices have been proposed. Since the dc path is isolated from the RF path, the three- and four-terminal switches allow for a simpler dc biasing, eliminating the need of expensive RF chokes and enable the optimization of the dc and RF performance separately. In this section, we present ReRAM, CBRAM, and PCM-based RF switches. For each of these technologies, we review the physical composition, performance, and their pros and cons.

A. CBRAM-Based RF Switches

The concept of using CBRAM devices as RF switches was first introduced by Nessel *et al.* [12], who presented a 10-μm gapless-type CBRAM switch with Ag and Ni electrodes. The device was measured up to 6 GHz, achieving below 0.5-dB IL and above 30-dB IS. Although R_{ON} and C_{OFF} are not reported, they can be approximated from the reported IL and IS values, leading to $R_{ON} = 6$ Ω, $C_{OFF} = 9$ fF, and thus $f_{CO} = 2.95$ THz. The set and reset voltages are, respectively, 1 and −1 V. The compliance current, both for set and reset, is 10 mA.

Another type of CBRAM RF switch is a gap-type switch [13], where the Ag and Au electrodes (active and inert, respectively) are separated by a 35-nm air gap, as shown in Fig. 6(a). The device is fabricated over a SiO_2 surface in a high resistivity silicon substrate (HRSi), in-line with a coplanar waveguide transmission line. The reported device presents an IL of approximately 0.3 dB and an IS of over 30 dB at 40 GHz. The reported R_{ON} is 2.6 Ω, R_{OFF} is approximately 1 TΩ, and C_{OFF} is on average 1.41 fF, leading to a typical cutoff frequency of 35 THz. In this device, $V_{SET} = 3$ V and $V_{RES} = -0.4$ V. The reported power-handling capabilities of this switch is 50 mW, at which the device starts to self-switch. The IP3 of this CBRAM RF switch is beyond 45 dBm.

To accurately predict the steady-state behavior of this device, a scalable lumped model was presented [55], [56], as shown in Fig. 6(c). The model is divided into analytic and numerical submodels. The former consists of a set of closed-form expressions from which the value of the lumped components can be determined. The latter is used to fit the model with measurement data. The model can be used to design and simulate larger circuits comprising these CBRAM-based RF switches, as will be presented in Section V.

Recently, nonvolatile resistance has been observed in multilayer 2-D materials based on conventional MIM structures with varied transitional metal dichalcogenide (TMD)-based hybrids [66]. In [67], atomristors were introduced. This device has molybdenum disulfide (MoS_2) in the insulating layer. Due to their extremely low ON-resistance, these devices can be used as high-performance RF switches. In these devices, MoS_2 is sandwiched between Au electrodes. When a positive voltage is applied, Au oxidizes and Au^+ ions fill the sulfur vacancies, building a conductive path between the two electrodes, thus reducing the resistance. In [68], atomristors with extremely high FOM (70 THz) and very fast switching (15 ns) are introduced. Another atomristor RF switch was recently presented in [69]. This device uses a very thin (∼0.33 nm) hexagonal boron nitride (hBN) as the insulating layer, and an FOM of 43 THz is shown.

Like MOSFET switches, CBRAM RF switches also tradeoff between R_{ON} and C_{OFF}. A smaller gap reduces the filament length, lowering R_{ON} and improving the IL. Reducing the gap also reduces the switching time and switching energy [70]. However, a smaller gap increases C_{OFF} since the distance between the electrodes is reduced. Hence, the IS degrades considerably. The increased C_{OFF} can be compensated for by reducing the section (area) of the electrodes. Furthermore, two devices can be connected in parallel to reduce R_{ON}, and the section of the electrodes can be engineered to avoid an increase in the C_{OFF}. Because the switching mechanism in CBRAM is voltage-controlled [21], [71], the switching would not be affected by the parallel connection. Nevertheless, the scaling of the electrode is limited by the compliance current required to achieve the desired R_{ON}.

Another design tradeoff exists between the switching energy and R_{ON}. Since R_{ON} is inversely proportional to the compliance current, it must be increased to lower the R_{ON}. The larger the compliance current, the greater the switching energy and the lower the device endurance [72]. A big challenge in the design of RF circuits using CBRAM RF switches is to control the parasitic resistance surrounding the device. Since these devices require a compliance current circuit to prevent damage during set, some parasitic resistance will always be in series with the two-terminal CBRAM. Therefore, when the SET voltage is applied, a voltage divider is formed with the parasitic resistance.

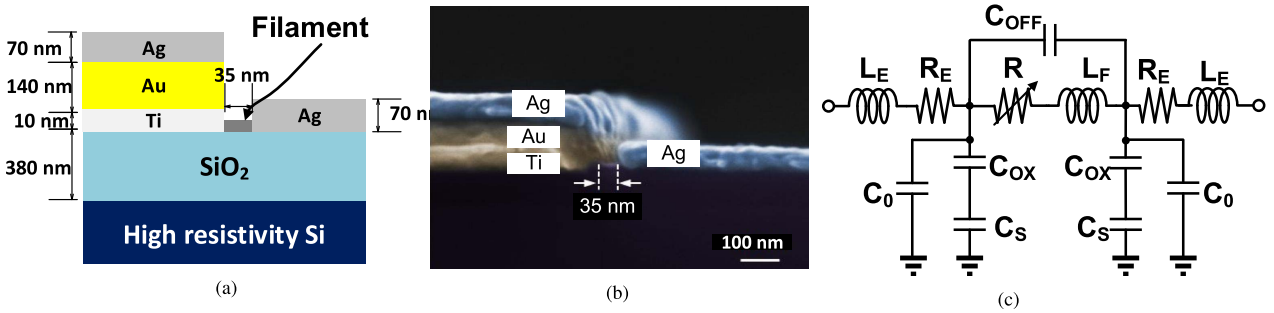

Fig. 6. *(a) Schematic cross section of the CBRAM-based RFMS proposed in [13]. Two metal electrodes (Ag and Ti/Au/Ag) separated by a 35-nm air gap in-line with the transmission line. (b) Cross-sectional false-colored SEM image of the device (adapted from [54]). (c) Lumped model proposed in [55] and [56], where R and C_{OFF} represent, respectively, the varying resistance and the gap capacitance (i.e., the capacitive coupling effect between the electrodes). Capacitor C_{OX} represents the SiO_2 parasitic capacitance, C_S the Si substrate capacitance, and C_0 the fringe capacitance between the signal line and ground planes. The inductance of the filament and the electrodes are also considered and are, respectively, L_F and L_E. The resistance R_E describes the losses in the electrodes.*

As R_{ON} is low, the voltage drop at the CBRAM can be lower than the required to set/reset. Hence, the parasitic must be kept as low as possible.

B. ReRAM-Based RF Switches

Oxide-based resistive switches have been extensively explored for memory and neuromorphic computing applications due to their analog switching properties. However, their applicability for RF switching has been limited since they typically have high ON-resistance states leading to unacceptably high IL. A reconfigurable passive planar absorber using ReRAM is theoretically proposed in [73], requiring an LRS of 300 Ω. These LRS values can be achieved by engineering TiO_x-based ReRAM devices [74]. However, more sophisticated RF circuitry requires RF switches with a much lower low-resistance state for reduced IL.

The first experimental results of an RF oxide ReRAM switch for the *X*-band using heavily reduced TiO_x 30 nm thick as active material [see Fig. 7(a)] is presented in [74]. The device was fabricated using a coplanar waveguide design with 100-μm signal linewidth and 60-μm gaps to ground to ensure 50-Ω impedance matching. The device is fabricated on an HRSi wafer substrate. Three photolithography steps were performed using an MA6 Suss MicroTec mask aligner and lift-off. To reduce the device dimensions below the resolution limit and thus lower the capacitance, the top electrode (TE) is misaligned from the BE, sacrificing some of the yield. The smallest obtained working device has a ~0.5-μm^2 area [see Fig. 7(b)]. After the lithography for the TE, a 30-nm TiO_x film is deposited by e-beam deposition in vacuum from TiO_2 pellets, followed by electrode metal deposition. This method ensured a clean interface between the TiO_x layer and TE.

The as-fabricated devices show a highly conductive, almost linear behavior, with resistances around 38 Ω at 0.05 V. The devices have low switching voltages (1 V). The maximum OFF-resistance is 35 kΩ, while the minimum ON-resistance is measured as 28 Ω. The switches could be switched at least 20 times at room temperature in air environment. Attempts to use higher set currents to further reduce the ON-resistance lead to irreversible device damage. The switch shows good IL (−2.1 dB) and isolation (−32 dB) at 10 GHz [see Fig. 7(c)]. The nonvolatility of these devices compares to similar devices, reported previously for other purposes [17]. The devices switch reliably for tens of cycles, showing better endurance than previously reported CBRAM RF switches [13]. Through device engineering, these devices might yield high endurance and improved performance. Other types of oxides materials, such as TaO_x [75] or multimaterial stacks [76], have exhibited smaller variability from switching cycle to cycle and thus greater endurance than TiO_x [77]. This opens up the possibility for oxide ReRAM RF switches with endurance higher than 10^6 cycles. Advanced nanolithography techniques can be used to reduce the device area even further to improve the isolation. Thinning the active layer combined with material engineering can help decrease further the ON-resistance and reduce the IL.

C. PCM-Based RF Switches

Some alloys of GST chalcogenides, for example, germanium telluride (GeTe) and antimony telluride (Sb_2Te_3), exhibit low resistivity in the crystalline phase, a critical requirement for RF switches. Their resistivity can be more than an order of magnitude lower than that of FETs [14], allowing for lower R_{ON} with similar or smaller feature size. The resistance in the amorphous state is sufficiently large to achieve an R_{OFF}/R_{ON} ratio higher than 10^4.

Two-, three-, and four-terminal PCM RF switches have been proposed [14], [45], [78]. Two-terminal devices are directly heated, that is, the thermal actuation is performed through the same electrodes where the RF signal flows in a similar operation as PCM. On the contrary, three- and four-terminal devices can be either heated directly or indirectly. In the latter, the thermal actuation path is isolated from

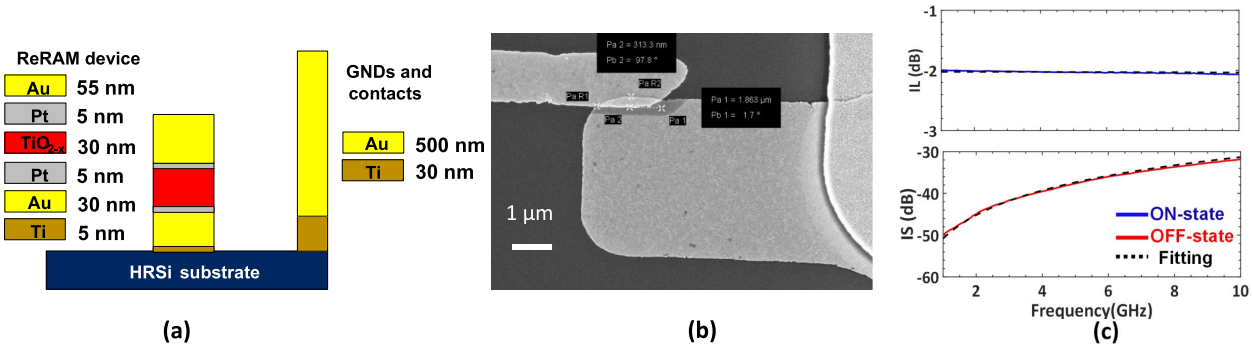

Fig. 7. *Oxide-resistive RF switch. (a) Schematic illustration showing a substoichiometric TiO_{2-x} oxide layer sandwiched between two metal electrodes (Pt). (b) Top view SEM photograph showing the low area $\sim 0.5\ \mu m^2$ due to intentional misalignment of optical features to reduce effective area in a low-cost manner. (c) Characterization results showing a measured IL of -2.1 dB and an IS of -32 dB at 10 GHz. Fitting is done using the model presented in [55] and [56].*

the RF transmission path. Note that thermal actuation and RF transmission requirements differ. For thermal actuation, refractory metals or alloys (e.g., W, Ta, and NiCr) are required because of their resistance to heat. However, these metals have larger electrical resistance than Cu, Al, or Au, which are the preferred choice for RF electrodes. Hence, two-terminal devices have an intricate tradeoff between thermal efficiency and RF performance. As in any RF switch, the isolation is determined by the C_{OFF}, which is mainly set by the parallel plate capacitance between the RF electrodes, and in the case of independent heaters, the coupling capacitance also contributes to the OFF-capacitance.

Besides electrothermal actuation using voltage or current pulses, optical switching of inline PCM RF switches using short UV laser pulses (~30 ns) has been proposed [79], [80]. To crystallize the PCM, a single laser pulse with a fluence (pulse energy divided by the laser surface spot) of 85–90 mJ/cm^2. To amorphize back the PCM, a second laser pulse having a much higher fluence of 185 mJ/cm^2 is used. Here, we will focus on electrically activated devices, which are those who can actually be integrated to RF integrated circuits (RFIC) front-ends.

1) Two-Terminal PCM Switches: In [78], a $3 \times 3\ \mu m^2$ two-terminal via switch [see Fig. 8(a) and (b)] with $R_{\text{ON}} = 1.8\ \Omega$ and $C_{\text{OFF}} \simeq 15$ fF is presented. The device is not a typical mushroom cell as the GeTe is sandwiched between two electrodes without the thin heater inside an insulation layer [as in Fig. 2(c)]. The FOM of this device is 5.9 THz, better than a large silicon-on-insulator (SOI) FET [81]. In this vertical device, C_{OFF} is determined by the parallel plate capacitance between the two electrodes. Because of the high relative permittivity (ε_r) of the PCM, C_{OFF} is large, which diminishes the IS of the device. To set this device, a pulse of 1.2 V must be applied for 5 μs. On the contrary, the reset pulse can be 500 ns wide with an amplitude of 3.5 V. This device exhibits high linearity, with an IP3 of 33 dBm and a $P_{1\text{ dB}}$ of 20 dBm.

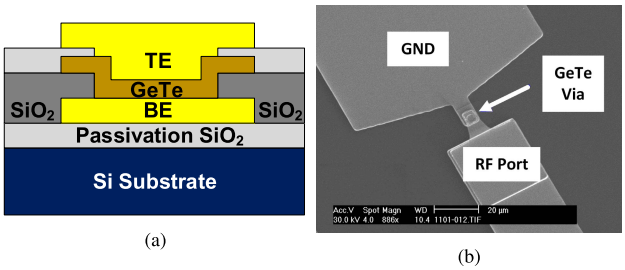

Fig. 8. *Directly heated two-terminal PCM-based RF switch. (a) Schematic cross section and (b) SEM cross section (taken from [78]).*

In [82], a two-terminal in-line PCM RF switch is presented. The GeTe layer is backside contacted using AlCu contacts. Thanks to the in-line configuration, a lower C_{OFF} (7 fF) is achieved, leading to an FOM of 22 THz. The key feature of this device is that switching in both directions is performed with short pulses (60 ns). Thus, reducing the switching energy by at least one order of magnitude compared to the indirect heating devices. This evidences the inherent tradeoff between energy efficiency and dc-RF isolation existing between the direct and indirect heating schemes.

2) Three-Terminal PCM RF Switches: A three-terminal PCM RF switch is presented in [45]. The switch is used to shortcut the signal line and the ground planes in a coplanar waveguide. The device consists of two vertical $1 \times 1\ \mu m^2$ GeTe via stacks, where the BE is shared by both stacks and the TE is connected to the ground plane [see Fig. 9(a) and (b)]. Since the BE is shared and the TE is connected to ground, the two PCM via stacks are in a parallel configuration. The achieved R_{ON} is 0.8 Ω, while C_{OFF} is 6.5 fF, meaning an FOM of 30.6 THz. The fabrication process is as follows: a blanket metal is deposited to build the BE. Then, GeTe is sputtered and patterned to form two via stacks

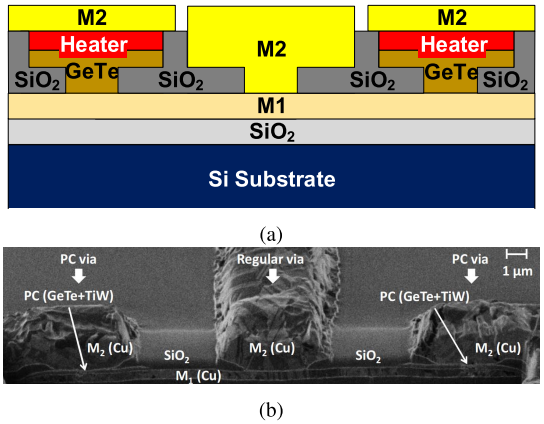

Fig. 9. *Directly heated three-terminal PCM-based RF switch. (a) Schematic cross section and (b) SEM cross section (taken from [45]).*

below the ground plane. Titanium tungsten (TiW) is used as a heater layer on top of the PCM to assist the thermal actuation, and the TE is deposited. Finally, the ground plane and the signal line (S) are metalized.

Because of the parallel connection, the resistance is half the resistance of the two-terminal device. In this case, the capacitance is also lower since the electrode section of each via is $1 \times 1\ \mu\text{m}^2$. Nonetheless, the fringe capacitance between the center electrode and the external electrode increases the C_{OFF} in this device. Because the programming is done simultaneously to both PCM via stacks, the three-terminal device requires pulses of up to 9 V to amorphize and 1.5 V to crystallize [83].

3) Four-Terminal PCM RF Switch: The four-terminal PCM RF switch using an independent heater, as shown in Fig. 10(a), was first introduced in [14]. The device is fabricated in-line with the RF paths, where the two RF electrodes are laterally connected to the phase-change material. The programming path (heater) is routed underneath the phase-change material and is isolated from the RF path by a dielectric thermal barrier. Therefore, C_{OFF} is mainly determined by the lateral gap between the RF terminals, reducing considerably the capacitance. Furthermore, with an independent heater, RF and thermal actuation paths can be optimized separately. However, indirect heating poses the problem of an increased energy to amorphize and crystallize as some of the heat will be dissipated on the thermal barrier. This device presents several advantages for RF circuit designers since many transistor-based applications rely on a control terminal, isolated from the RF signal. Thus, this device can replace the FET RF switch with ease.

The first generation of in-line four-terminal PCM RF switches with an independent heater achieved $R_{\text{ON}} = 8.35\ \Omega$ and $C_{\text{OFF}} = 18$ fF [14]. The relatively high resistance is because of the large gap between the RF terminals, high contact resistance, and high sheet resistance of GeTe. Developments in the fabrication process, for example, layer planarization, damascene metal processes, and improvements in etching process, have improved these devices [84], [86]–[88], leading to $R_{\text{ON}} = 0.9\ \Omega$, $C_{\text{OFF}} = 14.1$ fF, and FOM of 12.5 THz. The linearity of the device has also improved, with an IP3 of 72 dBm. Furthermore, Moon *et al.* [89] proposed the use of Sb_7Te_3 instead of GeTe, which drastically improves the device endurance and reduces switching energy consumption, achieving more than 10^7 switching cycles and less than 3 $\text{nJ}/\mu\text{m}^2$ per switch [90]. The transmission properties of such a device are also state of the art, with an FOM of 6.3 THz.

In the indirect heating scheme, the amorphization voltage can be as high as 10 V because of the high energy required to indirectly heat the PCM layer. Thus, the switching energy for crystallization and amorphization are 500 and 100 nJ, respectively. Conversely, in the direct heating scheme [see Fig. 10(b)], the energy required to crystallize is 7.5 nJ, and to amorphize 40 nJ. As mentioned, the direct heating scheme is more optimal for thermal actuation, but achieves lower RF performance, with an FOM of 4 THz.

D. Comparison Between Resistive Memory RF Switches

Despite dissimilar physical operation, materials, and structures, resistive memories achieve state-of-the-art FOM of RF switches. The best transmission parameters are achieved by the in-line four-terminal PCM RF switch with GeTe [91] and the 2DM CBRAM-based [68]. In the PCM RF switch, the resistivity of the phase-change material (GeTe or Sb_7Te_3) can be as low as $3 \times 10^{-6}\ \Omega \cdot \text{m}$ [86], thus allowing for a low R_{ON}. The in-line structure reduces the parasitic OFF-capacitance because of a smaller section. The CBRAM conducts through a metallic filament, thus a low R_{ON} is achieved. Again, the in-line (or lateral) structure decreases the parasitic capacitance of the device. Four-terminal devices are preferred in terms of transmission performance but are less energy-efficient. A comparison in terms of the FOM between the different resistive memory-based RF switches is listed in Table 2.

In terms of endurance, the in-line four-terminal PCM RF switch presented in [89] exhibits, so far, the highest among resistive RF switches for switching cycles ($>10^7$). This device uses Sb_7Te_3 as the phase-change material, which seemingly provides better reliability and lower energy consumption, thanks to lower melting temperature and better thermal design [90]. As for area, the ReRAM-based device and the CBRAM based on 2-D materials exhibit the smallest footprint. The switching voltages vary among the different technologies, from less than 1 V to over 10 V. The ReRAM- and CBRAM-based devices require voltages in the 1-V range, while the indirectly heated PCM RF switches may require voltages as high as 10 V [86], [87]. Directly heated PCM RF switches require voltages in the 3–7-V range. The switching time also varies among the

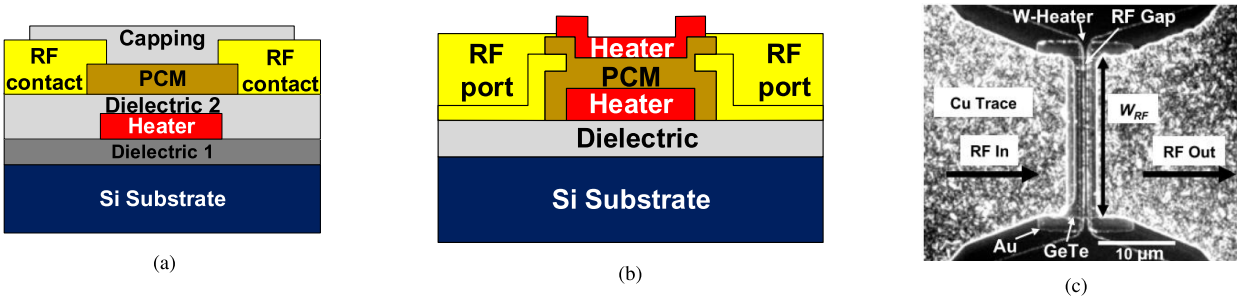

Fig. 10. *Schematic illustration of in-line four-terminal PCM RF switch with (a) indirect heating [84] and (b) direct heating [85]. (c) SEM image of an indirectly heated in-line four-terminal PCM RF switch with indirect heating (taken from [86]).*

Table 2 Comparison of the FOM of Resistive Memory-Based RF Switches

Ref.	Technology	IL (dB)	IS (dB)	Band-width (GHz)	R_{ON} (Ω)	C_{OFF} (fF)	FOM (THz)	Area (μm^2)	Actua-tion[2] Voltage (V)	Power Handling (W)	Endurance[1] (#cycles)
[91]	2-terminal PCM	<0.2	>30	DC-67	0.7	4	57	10^3	N/A	10	N/A
[45]	3-terminal PCM	N/A	N/A	N/A	0.8	6.5	30.6	1	1.5	N/A	10
[82]	2-terminal PCM	<0.12	>15	DC-65	1	7	22	4.5	N/A	N/A	N/A
[87]	4-terminal PCM	<0.25	>10	DC-40	0.9	14.1	12.5	27	N/A	N/A	100
[86]	4-terminal PCM	0.1	>20	DC-14	1.4	15.4	7.4	8	8.4	5	N/A
[92]	4-terminal PCM	<0.3	>10	DC-40	1.2	18.1	7.3	27	N/A	3.15	$> 10^5$
[89]	4-terminal PCM	<1	>20	DC-50	4.5	5.6	5	88	6.5	N/A	$> 10^7$
[78]	2-terminal PCM	<1	>18	DC-25	1.8	15	5.9	4	3.5	5	N/A
[85]	4-terminal PCM	<0.5	>20	DC-20	3.9	10	4.1	7.2	9	>1	200
[14]	4-terminal PCM	<0.5	>10	DC-20	4.5	35	1.0	36	N/A	0.6	> 1500
[74]	ReRAM	<2	>32	DC-10	28	2	2.8	0.5	2	N/A	N/A
[68]	2DM CBRAM	<0.25	>29	DC-67	2.7	0.84	70	0.03	1	N/A	$> 10^3$
[69]	2DM CBRAM	<0.2	>15	DC-110	1.6	2.3	43	0.25	1.5	0.1	N/A
[13]	CBRAM	<0.3	>30	DC-40	2.6	1.45	42.2	0.6	3	0.1	$< 10^3$
[12]	CBRAM	<0.5	>35	DC-6	6	9	2.95	400	1	0.5	N/A

[1] Endurance reported in each work, not necessarily the maximum possible cycling of the technology.
[2] The maximum actuation voltage is taken.

different technologies. ReRAM and CBRAM have faster switching, theoretically below 10 ns. Conversely, indirectly heated PCM switches require 100 ns for amorphization and 1 μs for crystallization. The main performance metrics of the resistive memory RF switches are summarized in Table 1.

To be BEOL-compatible, the CBRAM switch would require diffusion barriers to prevent Ag or Cu contamination to the transistors. More "fab-friendly" materials such as W could be used instead of Au for the inert electrodes, which would slightly increase R_{ON}. The low deposition temperature of GeTe and Sb_7Te_3 allows the PCM switch to be compatible with the Cu-BEOL CMOS process, which requires temperatures below 400 °C. However, the large thickness of the interlayer dielectrics and their low thermal conductivity may prevent the PCM switch from quenching fast enough to prevent recrystallization. In [93], the problem is solved by adding AlN heating spreaders layer over a thick oxide that emulates the conditions of a real CMOS process. With this additional layer, the switch can be set and reset properly, proving the CMOS compatibility of these devices.

Table 3 RF Performance of Different RF Switch Technologies

Technology	IL[1] (dB)	IS[1] (dB)	Bandwidth (GHz)	FOM (THz)	Ref.
CMOS SOI 45 nm	<3	>15	110-220	0.88	[98]
CMOS SOI 180 nm	N/A	N/A	N/A	0.61	[81]
CMOS SOI 130 nm	<0.2	N/A	DC-10	1.38	[99]
GaAs pHEMT [2]	<0.5	>20	0.5-2.5	1.1	[100]
GaN SLCFET [3]	<0.6	>25	DC-20	1.2	[101]
AlGaAs PIN diode	<0.5	>20	0.05-50	2.4	[102]
VO_2 MIT	<0.4	>15	DC-15	2.1	[50]
Metal Contact RF MEMS	<1	>20	DC-40	3.8	[95]
Capacitive RF MEMS	< 0.3	> 20	20-35	N/A	[103]
ReRAM	<2	>32	DC-10	2.8	[74]
CBRAM	<0.3	> 30	DC-40	42.2	[13]
2DM CBRAM	<0.3	>15	DC-50	70	[68]
PCM	<0.2	>30	DC-67	57	[91]

[1] Taken at the maximum frequency.
[2] SP7T configuration.
[3] Series-shunt SPDT configuration.

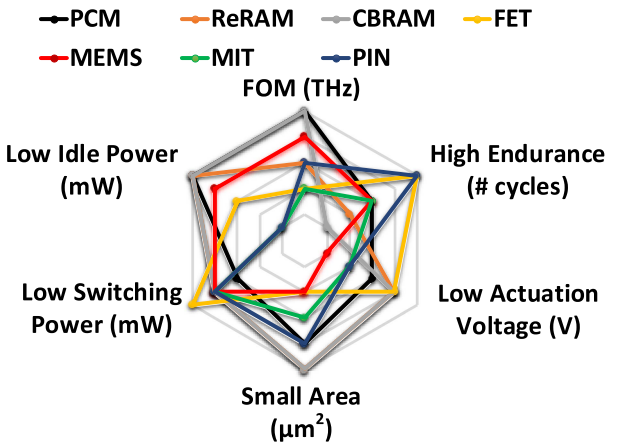

Fig. 11. *Qualitative metrics comparison of different technologies. Resistive memory-based RF switches exhibit high performance in most metrics, except for endurance due to their current immature/research-grade state.*

E. Comparison With Other RF Switch Technologies

Resistive memory RF switches achieve better FOM than FETs, and similar (or even better) FOM than MEMS, but with smaller footprint. However, FET switches are still faster and have higher endurance. The FOM of MOS devices remains lower than 1 THz [94], while MEMSs have achieved an FOM over 17 THz [95]. Compound semiconductor FETs (e.g., InP, GaAs, and GaN) achieve higher FOM, power handling, and faster switching than CMOS [96], [97]; however, they are expensive and not very suitable for logic circuits. This undermines the possibility of implementing a monolithically integrated radio transceiver including the baseband digital blocks. Despite their excellent FOM, the adoption of MEMS in the RF market has been hindered by their high cost, high actuation voltages (5–80 V), and reliability issues, for example, dielectric charging and contact interface degradation [9], [58]. The high FOM of p-i-n diodes contrasts with their high static power, low power handling, and poor integration characteristics. The FOMs of resistive memory-based RF switches and other technologies are compared in Table 3.

Although CMOS and BiCMOS can provide intercircuit reconfiguration (i.e., between different narrowband blocks in the system), they cannot provide reconfiguration in narrowband circuits because of their large parasitics. Wideband circuits are an alternative approach for multiband front-ends. Still, narrowband circuits outperform their wideband counterparts. With a high FOM, ease of integration, low footprint, low switching energy, and relatively high power handling, resistive memory RF switches may emerge as the enabler and catalyst of reconfigurable wireless communication systems. As a drawback, the endurance of these nonvolatile switches is limited, among others, by the volume expansion of the material (in PCM RF switches) or contact degradation (in CBRAM and ReRAM) due to oxidation of the electrode. Thus, the final adoption by the industry depends on improvements in their reliability and manufacturing costs. Ten million cycles, as shown in [89], is an excellent starting point. Nonetheless, these technologies require further improvements both in material science and processing. A summarizing comparison between the different technologies is shown in Fig. 11.

V. APPLICATIONS OF RESISTIVE MEMORY-BASED RF SWITCHES

A reconfigurable radio will consist of adaptive or tunable blocks (i.e., intracircuit reconfiguration), or of radio chains where the connection between different blocks can be changed (i.e., intercircuit reconfiguration), or a mix of both schemes (intra–inter-circuit reconfiguration). Possible applications of high-performance RF switches based on resistive memory devices are listed in Table 4. All these application require high-performance, small footprint RF switches. As previously discussed, three- and four-terminal devices present the advantages of built-in isolation between the programming and RF paths. Two-terminal CBRAM, ReRAM, and PCM-based RF switches may be suitable for intracircuit reconfiguration (as shown in Section V-B), but less effective for intercircuit reconfiguration since the control circuit must provide the dc-RF decoupling. This may lead to large-area overheads, thus reducing the advantages of their small footprint.

Certainly, endurance is a major concern to adopt these technologies in RFIC. For instance, a reconfigurable

Table 4 Applications of Resistive Memory-Based RF Switches

Fundamental Elements	
Element	**Requirements**
Tunable inductor Tunable capacitor Multiplexers Tunable antenna	• Low R_{ON}, low C_{OFF} • Endurance $> 10^6$ • BEOL-compatible
RF Front-End Subsystems	
Subsystem	**Requirements**
Switching networks Tunable attenuators Tunable filters Switched antenna Phase-shifters Switched matching networks Switched oscillators, amplifiers	• Low R_{ON}, low C_{OFF} • Small footprint • Endurance $10^6 - 10^9$ • Low biasing circuit overhead
RF Front-End Systems	
System	**Requirements**
Reconfigurable radio	• High-performance RF switch • Small footprint • Multiple switching networks
Phased-array	• Low-loss phase-shifters • Small footprint switches
Constrained power/energy radio	• Low-power switching • Low static energy

wireless communication system would require between 0.01 and 4 billion cycles, while a phased-array radar system would require more than 10 billion cycles [9]. These emerging nonvolatile devices used for digital memory applications have shown promise of high endurance in research settings, with some devices exhibiting >1 billion cycles—reported 10^9 for PCM-based devices [42] and 10^{12} for ReRAM-based devices [35]. Currently, these results seem to be for champion devices and resistive memory RF switches still do not achieve that endurance. However, device variability is a well-known issue for emerging technologies in general. It is expected that as the resistive RF switches will move from research laboratories to industry-level fabrication facilities, statistical characterization of high volumes of devices will enable better understanding of the failure modes while improved control of the material and fabrication properties is expected to reduce the device variability. While these emerging technologies have the potential to achieve the required endurance, in the long term, their currently limited endurance may be enough for a system intended to be reconfigured only a few times.

In this section, we present examples of reconfigurable circuits using resistive memory-based RF switches. We focus on intracircuit configuration, where the performance of the block can be changed to suit the requirements of widely separated frequency bands, such as tunable inductors, antennas, and filters. We also present some works on basic switching networks basic circuits, for example, single-pole double-throw (SPDT), DPDT, omnidirectional eight-port switch.

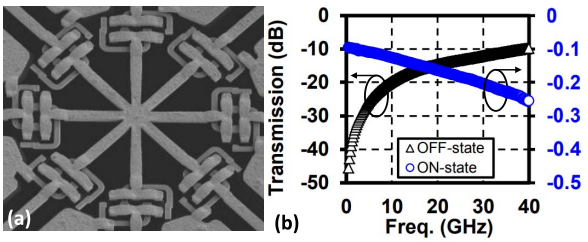

Fig. 12. *(a) SEM image of the eight-port omnidirectional IPCS switch matrix. (b) Performance of an SPST device in the matrix. Taken from [106].*

A. Switching Matrix Blocks

A series-shunt SPDT based on GeTe-IPCS is presented in [104]. The SPDT exhibited IL < 1.1 dB and IS > 39 dB in the dc-65-GHz bandwidth. Furthermore, 30 000 switching cycles were demonstrated with low variation in the IL (<0.05 dB) and in the IS (<2 dB). The switch area is as small as (0.33 × 0.61 mm^2). In [105], an DPDT switch with IL below 4 dB and IS better than 15 dB at 20 GHz is presented.

Four-port and eight-port omnidirectional switches are presented in [106]. The areas of the four- and eight-port switches are 1.3 and 1.7 mm^2, respectively. Several of these switches are 3-D integrated with an SiGe radio transceiver containing banks of amplifiers, IF downconverters, bandpass filters, among others. With the omnidirectional switches, the radio transceiver can be reconfigured for an iridium system or a common data link (CDL) receiver. An SEM image of the eight-port omnidirectional IPCS switch is shown in Fig. 12(a), while the RF performance of the SPST is shown in Fig. 12(b).

In [107], a dc-67-GHz monolithically integrated redundancy switch matrix using T-type switches is presented. The redundancy switch is implemented using two cascaded 4 × 6 IPCS T-type switches [see Fig. 13(a)], showing an IL < 3 dB and IS > 20 dB among dc-67 GHz [see Fig. 13(b) and (c)]. This switch has a footprint of 0.88 × 1.1 mm^2.

B. Tunable Inductors

In a resistive memory array, the devices are built in a crossbar manner (namely, in the junction between two adjacent metal layers, perpendicularly routed). Since RF inductors are fabricated using a wire loop with a cross-under layer to provide access to the second electrode, a resistive memory RF switch could be placed between the two layers. In [108], a CBRAM switch is proposed as a switching via, which can change the effective length (or the number of loops N) of the inductor (see Fig. 14), thus changing the inductance of the inductor. The simulation results show that the inductance can be tuned from 2.3 to 9.6 nH with a quality factor (Q-factor) varying between 12.4 and 18, respectively, for ON-state and OFF-state.

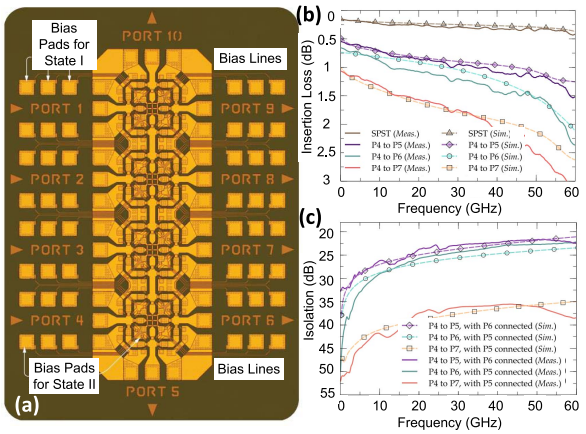

Fig. 13. *(a) Redundancy switch matrix using cascaded T-type switching unit cells. Simulated and measured (b) IL and (c) IS of the redundancy switch over dc-67 GHz (taken from [107]).*

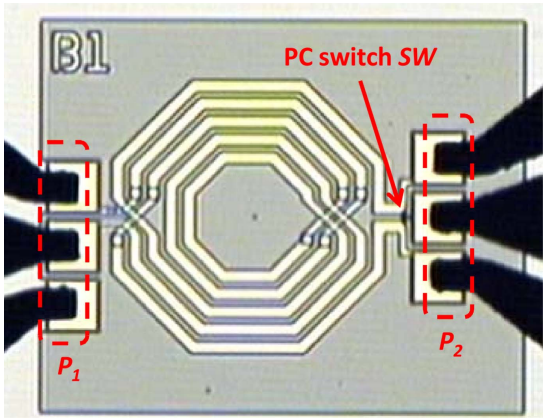

Fig. 15. *Reconfigurable RF inductor using three-terminal RF switch [83].*

In [83], a reconfigurable RF inductor using three-terminal PCM switches is proposed. It consists of a primary and a secondary winding, L_1 and L_2, respectively, which are routed in an interleaved manner. The terminals of L_2 are connected to the three-terminal PCM switch (see Fig. 15). When the switch is ON, current flowing through L_2 creates a magnetic field that opposes that of L_1, reducing the total inductance seen from port 1 (P1). Contrarily, when the PCM switch is in the OFF-state, no current flows through L_2 and the total inductance is that of L_1 only. This way, the inductor is tuned between 0.9 and 1.9 nH with a Q-factor varying from 5.8 to 12.4, respectively, for the OFF- and ON-states.

C. Reconfigurable Antennas and Filters

GeTe IPCSs are used in [109] to tune the antenna aperture of a dipole array. The IPCSs are optically controlled using short laser pulses, which are fed using a single-mode optical fiber. The dipole array can be tuned within the 0.5–4.0-GHz frequency range. The bandwidth can be dynamically controlled using GeTe IPCSs built between the radiating elements. When the IPCSs are in the crystalline state, the radiating elements form a connected dipole array. Contrarily, when the IPCSs are in the amorphous state, a nonconnected dipole array is created. In [110], a reconfigurable patch antenna using a phase-change material parasitic patch is presented. The feed line is connected to a metallic patch with can be coupled to either none, one, or two phase-change parasitic patches, thus changing the radiation pattern of the antenna by tilting the beam accordingly. As in [109], the phase change is done optically using short laser pulses.

A reconfigurable bandpass filter for the X-band is presented in [111]. The filter consists of two $\lambda/2$ microstrip line open-loop resonators, each loaded with a switchable capacitor switched by a four-terminal PCM switch at the end. When the PCM switches are ON, the lower frequency passband of 7.45 GHz is achieved, with an IL of 3.2 dB, 3-dB bandwidth of 482 MHz, and return loss larger than 30 dB. Contrarily, when the switches are OFF, the filter is switched to the higher frequency band (8.07 GHz), presenting an IL of 2.6 dB, bandwidth of 520 MHz, and return loss better than 18 dB.

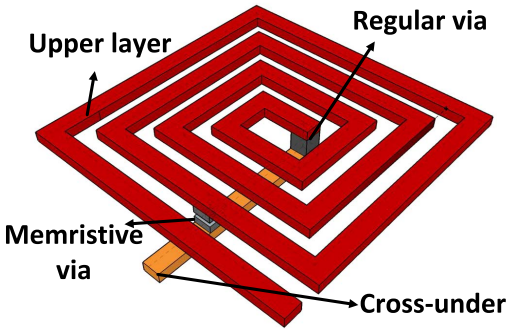

Fig. 14. *CBRAM via switched tunable inductor [108]. A CBRAM RF switch is placed between the upper layer and the cross-under of the inductor to tune the inductance.*

D. Dual-Band Low-Noise Amplifiers

Low-noise amplifiers (LNAs) have a fundamental role in the global performance of radio transceivers as they are usually the first active stage after the antenna in a receiver [112]. In adaptive systems, the LNA must provide low noise figure (NF), high gain, and good input matching for multiple frequency bands. LNAs supporting multiple bands consist of various switchable amplification transistors, capacitors, and/or inductors. Therefore, high-performance RF switches are critical components for multi-band LNAs, and resistive memory-based RF switches are excellent candidates to provide the required performance.

A dual-band LNA using a four-terminal indirectly heated PCM RF switch and CMOS 0.13-μm CMOS technology is presented in [113]. The LNA consists of two common sources with source degeneration which are switched with the PCM RF switch (see Fig. 16). The LNA achieves high gain, 19.5 and 20 dB, and low NF, 2.85 and 2.86 dB, for 3 and 5 GHz, respectively. The penalty of using the switch, compared to the single CMOS LNA, is less than 2 dB in gain and 1 dB in NF.

In [114], simulations of a dual-band CMOS LNA using CBRAM-based tunable inductors [108] are presented. This design uses only a single common source with inductive source degeneration for both bands. Two tunable inductors are used to provide the matching and stability conditions for 2.4 and 5 GHz, one at the input and one at the output of the amplifier. The LNA is designed using a 0.18-μm RF CMOS technology and achieves a gain of 18.8 and 10.3 dB at 2.4 and 5 GHz, respectively, and an NF below 2.3 dB at both bands.

E. Reconfigurable Voltage-Controlled Oscillator

Integrated voltage-controlled oscillator (VCOs) are fundamental blocks in radio transceivers. They are used as local oscillators in frequency synthesizers to provide local carriers for signal modulation [115], [116]. Therefore, the performance of the VCO is critical to the overall performance of the radio. The main design issues are oscillating frequency, phase noise (i.e., fluctuations in the phase of the signal due to jitter), output power level, and frequency tuning range [115], [117].

Two topologies of multiband VCOs are presented in [45]. A classic *LC* cross-coupled VCO is loaded with a switchable inductor using PCM RF switch in two configurations: series-connected (SC) and coupled-controlled (CC) (see Fig. 17). The switchable inductors considerably increase the frequency tuning range of the VCO, as they allow to synthesize carriers of widely separated frequency bands. The SC topology uses a PCM RF switch to bypass a portion of the inductor, thus changing the inductance seen by the VCO. Contrarily, the CC topology uses the dual winding inductor described in Section V-B.

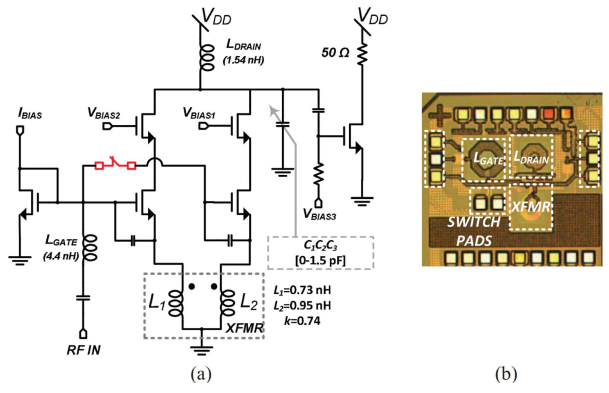

Fig. 16. *(a) Schematic and (b) die optical image of a dual-band LNA (taken from [113]).*

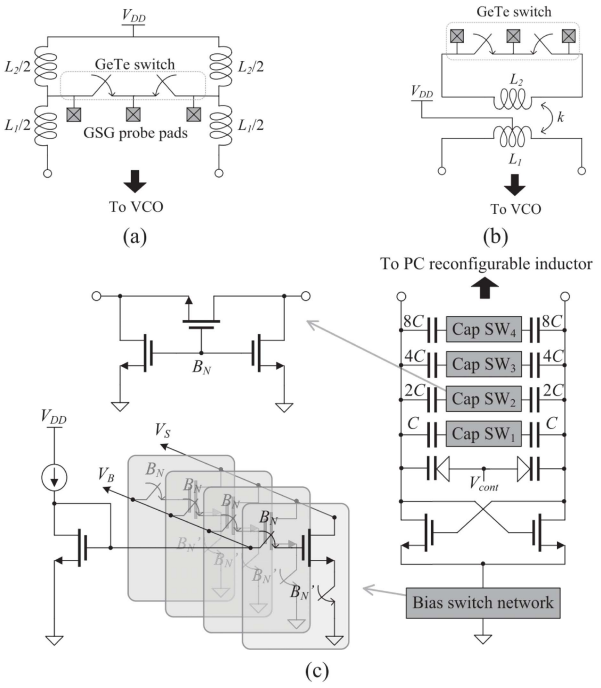

Fig. 17. *(a) SC and (b) CC schemes. (c) Schematic of the cross-coupled LC VCO using switchable inductor based on the PCM RF switch (taken from [45]).*

The VCO is fabricated in 0.13-μm CMOS technology, while the PCM was fabricated using an in-house fabrication process and was integrated using a custom flip-chip integration process. Wide tuning ranges of 2.89–4.23 (4.93–7.79) and 4.80–8.53 (5.28–10.20) GHz is achieved for OFF-/ON-states for the SC (CC) topology. The phase noise over the tuning range is lower than −103.4 and −102.7 dBc/Hz, at a 1-MHz offset frequency.

VI. CONCLUSION

High-performance RF switches based on resistive memory technologies have achieved several breakthroughs in the last few years: state-of-the art FOM, smaller footprint compared with standard technology, fast switching, and high endurance. These switches are thus major candidates for new adaptive RF circuits. These adaptive circuits will serve as the basic building blocks for multiband/multistandard radio transceivers. In this article, we reviewed resistive memory-based RF switch technologies, including CBRAM, PCM, and ReRAM.

Among resistive memory technologies, PCM has been most widely studied and has rapidly matured in recent years. Particularly, the four-terminal indirectly heated PCM RF switch has demonstrated several important milestones, such as state-of-the-art FOM (>10 THz), process stability, high endurance (>10^7), and isolated paths for RF and dc. Moreover, integration with CMOS and compound

semiconductors has already been demonstrated and the basis for monolithic integration with standard process is being researched. Notwithstanding, further improvements are required for a final deployment of this technology in actual systems. For instance, increasing the endurance is compulsory for phased arrays and reconfigurable systems, and the switching energy and actuation voltage of PCM-based RF switches must be reduced to ease their integration with CMOS. While PCM RF switches are the most widely studied at this time, CBRAM and RRAM have performance advantages like lower area, lower switching voltages, and faster speed, so future advancements in RF switches based on these technologies are expected.

The accelerated pace at which these technologies are being developed is promising and the open issues should be solved in the near future, especially as they move from research laboratories to industry-level fabrication facilities. We have identified several critical research lines toward the implementation of high-performance RF switches based on resistive memories.

1) *Scaling limits:* Reducing the dimensions of the devices is critical to improve the density in phased-array systems and reconfigurable circuits. Furthermore, as the switching energy is strongly dependent on the volume and/or lateral dimensions of the device, scaling is desired to reduce their energy consumption. However, further reduction of the specific and contact resistivity is a challenging goal. Also, C_{OFF} places a lower boundary on the physical dimensions of the device, if a large IS is desired.
2) *Material exploration:* New materials may enable higher energy efficiency, lower switching energy, and higher endurance. For instance, the performance of the atomristor can be improved by exploring different TMD and electrode materials, while playing with the doping concentrations. Since Au is not a popular metal in standard transistor processes, another metal for the electrodes is required. For CBRAM, Ag-based electrodes should be replaced by Cu-based electrodes to allow for integration with standard CMOS.
3) *Application-oriented optimization:* With few exceptions, most of the research to date has focused on the device level. Circuit design with these technologies will require application-specific optimization of the device, either to achieve lower IL, higher IS, lower energy consumption, or faster switching, depending on the circuit specifications.

The rapid growth in the number of the mobile communication devices and the great diversity of the communication standards will require reconfigurable radios that can adapt to widespread frequency bands, while providing the required IL, IS, gain, linearity, and stability. Resistive memories have already shown promising performance that could make them the basic building block for these reconfigurable RF systems. Improvements in endurance are expected from process enhancements when porting these technologies to industry-level foundries. Their ease of fabrication and purely solid-state operation would enable them to be integrable on a variety of rigid and flexible substrates. Their integration with standard transistor processes will open a whole new world of opportunities in the semiconductor industry for dense, low-energy, multistandard radios. ■

REFERENCES

[1] D. Evans, "The Internet of Things—How the next evolution of the Internet is changing everything," Cisco, San Jose, CA, USA, White Paper, 2011, vol. 1, no. 2011.

[2] T. Sowlati *et al.*, "Single-chip multiband WCDMA/HSDPA/HSUPA/EGPRS transceiver with diversity receiver and 3G DigRF interface without SAW filters in transmitter/3G receiver paths," in *IEEE Int. Solid-State Circuits Conf. (ISSCC) Dig. Tech. Papers*, Feb. 2009, pp. 116–117.

[3] T. Georgantas *et al.*, "A 13 mm^2 40 nm multiband GSM/EDGE/HSPA+/TDSCDMA/LTE transceiver," in *IEEE Int. Solid-State Circuits Conf. (ISSCC) Dig. Tech. Papers*, Feb. 2015, pp. 1–3.

[4] Apple Inc. (2018). *iPhone X*. [Online]. Available: https://www.apple.com/iphone-x/specs/

[5] Y. Lin *et al.*, "SODA: A low-power architecture for software radio," *ACM SIGARCH Comput. Arch. News*, vol. 34, no. 2, pp. 89–101, May 2006.

[6] K. Tan, H. Liu, J. Zhang, Y. Zhang, J. Fang, and G. M. Voelker, "Sora: High-performance software radio using general-purpose multi-core processors," *Commun. ACM*, vol. 54, no. 1, pp. 99–107, Jan. 2011.

[7] M. Rais-Zadeh, J. T. Fox, D. D. Wentzloff, and Y. B. Gianchandani, "Reconfigurable radios: A possible solution to reduce entry costs in wireless phones," *Proc. IEEE*, vol. 103, no. 3, pp. 438–451, Mar. 2015.

[8] X. S. Wang and C. P. Yue, "A dual-band SP6T T/R switch in SOI CMOS with 37-dBm $P_{-0.1dB}$ for GSM/W-CDMA handsets," *IEEE Trans. Microw. Theory Techn.*, vol. 62, no. 4, pp. 861–870, Apr. 2014.

[9] G. M. Rebeiz, *RF MEMS: Theory, Design, and Technology*. Hoboken, NJ, USA: Wiley, 2003.

[10] C. M. Ta, E. Skafidas, and R. J. Evans, "A 60-GHz CMOS transmit/receive switch," in *IEEE Radio Freq. Integr. Circuits Symp. Dig. Papers*, Jul. 2007, pp. 725–728.

[11] K. M. Naegle, S. Gupta, and D. J. Allstot, "Design considerations for a 10 GHz CMOS transmit-receive switch," in *Proc. IEEE Int. Symp. Circuits Syst.*, Jul. 2005, pp. 2104–2107.

[12] J. A. Nessel, R. Q. Lee, C. H. Mueller, M. N. Kozicki, M. Ren, and J. Morse, "A novel nanoionics-based switch for microwave applications," in *IEEE MTT-S Int. Microw. Symp. Dig.*, Jun. 2008, pp. 1050–1054.

[13] S. Pi, M. Ghadiri-Sadrabadi, J. C. Bardin, and Q. Xia, "Nanoscale memristive radiofrequency switches," *Nature Commun.*, vol. 6, no. 7519, pp. 1–9, Jun. 2015.

[14] N. El-Hinnawy *et al.*, "A four-terminal, inline, chalcogenide phase-change RF switch using an independent resistive heater for thermal actuation," *IEEE Electron Device Lett.*, vol. 34, no. 10, pp. 1313–1315, Oct. 2013.

[15] D. J. Wouters, R. Waser, and M. Wuttig, "Phase-change and redox-based resistive switching memories," *Proc. IEEE*, vol. 103, no. 8, pp. 1274–1288, Aug. 2015.

[16] M. Ramadan, N. Wainstein, R. Ginosar, and S. Kvatinsky, "Adaptive programming in multi-level cell ReRAM," *Microelectron. J.*, vol. 90, pp. 169–180, Aug. 2019.

[17] M. Prezioso, F. Merrikh-Bayat, B. D. Hoskins, G. C. Adam, K. K. Likharev, and D. B. Strukov, "Training and operation of an integrated neuromorphic network based on metal-oxide memristors," *Nature*, vol. 521, no. 7550, pp. 61–64, May 2015.

[18] L. Danial *et al.*, "Two-terminal floating-gate transistors with a low-power memristive operation mode for analogue neuromorphic computing," *Nature Electron.*, vol. 2, no. 12, pp. 596–605, Dec. 2019.

[19] H.-S. P. Wong *et al.*, "Phase change memory," *Proc. IEEE*, vol. 98, no. 12, pp. 2201–2227, Dec. 2010.

[20] H.-S. P. Wong, H.-Y. Lee, S. Yu, Y.-S. Chen, Y. Wu, P.-S. Chen, B. Lee, F. T. Chen, and M.-J. Tsai, "Metal-oxide RRAM," *Proc. IEEE*, vol. 100, no. 6, pp. 1951–1970, Jun. 2012.

[21] I. Valov, R. Waser, J. R. Jameson, and M. N. Kozicki, "Electrochemical metallization memories—Fundamentals, applications, prospects," *Nanotechnol.*, vol. 22, pp. 1–22, May 2011.

[22] D. Ielmini and R. Waser, *Resistive Switching: From Fundamentals of Nanoionic Redox Processes to Memristive Device Applications*. Hoboken, NJ, USA: Wiley, 2016.

[23] S. W. Fong, C. M. Neumann, and H.-S.-P. Wong, "Phase-change memory—Towards a storage-class memory," *IEEE Trans. Electron Devices*, vol. 64, no. 11, pp. 4374–4385, Nov. 2017.

[24] R. Waser and M. Aono, "Nanoionics-based resistive switching memories," *Nature Mater.*, vol. 6, no. 11, pp. 833–840, Nov. 2007.

[25] S. Kvatinsky *et al.*, "MAGIC—Memristor-aided logic," *IEEE Trans. Circuits Syst. II, Exp. Briefs*, vol. 61, no. 11, pp. 895–899, Nov. 2014.

[26] S. H. Jo, T. Chang, I. Ebong, B. B. Bhadviya, P. Mazumder, and W. Lu, "Nanoscale memristor device as synapse in neuromorphic systems," *Nano Lett.*, vol. 10, no. 4, pp. 1297–1301, Mar. 2010.

[27] H. Y. Lee *et al.*, "Low power and high speed bipolar switching with a thin reactive Ti buffer layer in robust HfO_2 based RRAM," in *IEDM Tech. Dig.*, Dec. 2008, pp. 1–4.

[28] J. J. Yang, D. B. Strukov, and D. R. Stewart, "Memristive devices for computing," *Nature Nanotechnol.*, vol. 8, no. 1, pp. 13–24, Jan. 2013.

[29] R. Meyer *et al.*, "Oxide dual-layer memory element for scalable non-volatile cross-point memory technology," in *Proc. 9th Annu. Non-Volatile Memory Technol. Symp. (NVMTS)*, Dec. 2008, pp. 1–5.

[30] C. J. Chevallier *et al.*, "A 0.13 μm 64Mb multi-layered conductive metal-oxide memory," in *IEEE Int. Solid-State Circuits Conf. (ISSCC) Dig. Tech. Papers*, Mar. 2010, pp. 260–261.

[31] A. C. Torrezan, J. P. Strachan, G. Medeiros-Ribeiro, and R. S. Williams, "Sub-nanosecond switching of a tantalum oxide memristor," *Nanotechnology*, vol. 22, no. 48, Nov. 2011, Art. no. 485203.

[32] B. J. Choi *et al.*, "High-speed and low-energy nitride memristors," *Adv. Funct. Mater.*, vol. 26, no. 29, pp. 5290–5296, May 2016.

[33] S. Yu, Y. Wu, Y. Chai, J. Provine, and H.-S.-P. Wong, "Characterization of switching parameters and multilevel capability in HfO_x/AlO_x bi-layer RRAM devices," in *Proc. Int. Symp. VLSI Technol., Syst. Appl.*, Apr. 2011, pp. 1–2.

[34] J. Liang and H.-S.-P. Wong, "Cross-point memory array without cell selectors—Device characteristics and data storage pattern dependencies," *IEEE Trans. Electron Devices*, vol. 57, no. 10, pp. 2531–2538, Oct. 2010.

[35] Y.-B. Kim *et al.*, "Bi-layered RRAM with unlimited endurance and extremely uniform switching," in *Symp. VLSI Technol.-Dig. Tech. Papers*, Aug. 2011, pp. 52–53.

[36] D. Ielmini, "Resistive switching memories based on metal oxides: Mechanisms, reliability and scaling," *Semicond. Sci. Technol.*, vol. 31, no. 6, May 2016, Art. no. 063002.

[37] W. Chen, S. Tappertzhofen, H. J. Barnaby, and M. N. Kozicki, "SiO_2 based conductive bridging random access memory," *J. Electroceram.*, vol. 39, nos. 1–4, pp. 109–131, Mar. 2017.

[38] M. Kund *et al.*, "Conductive bridging RAM (CBRAM): An emerging non-volatile memory technology scalable to sub 20 nm," in *IEDM Tech. Dig.*, Dec. 2005, pp. 754–757.

[39] E. Vianello *et al.*, "Resistive memories for ultra-low-power embedded computing design," in *IEDM Tech. Dig.*, Dec. 2014, pp. 6.3.1–6.3.4.

[40] R. Cao *et al.*, "Improvement of device reliability by introducing a BEOL-compatible TiN barrier layer in CBRAM," *IEEE Electron Device Lett.*, vol. 38, no. 10, pp. 1371–1374, Aug. 2017.

[41] S. Raoux, H.-Y. Cheng, J. L. Jordan-Sweet, B. Muñoz, and M. Hitzbleck, "Influence of interfaces and doping on the crystallization temperature of Ge–Sb," *Appl. Phys. Lett.*, vol. 94, no. 18, May 2009, Art. no. 183114.

[42] H. Y. Cheng *et al.*, "Novel fast-switching and high-data retention phase-change memory based on new Ga-Sb-Ge material," in *IEDM Tech. Dig.*, Dec. 2015, pp. 3–5.

[43] D. M. Pozar, *Microwave Engineering*. Hoboken, NJ, USA: Wiley, 2005.

[44] J. A. del Alamo, "Nanometre-scale electronics with III–V compound semiconductors," *Nature*, vol. 479, no. 7373, pp. 317–323, Nov. 2011.

[45] C.-Y. Wen, G. Slovin, J. A. Bain, T. E. Schlesinger, L. T. Pileggi, and J. Paramesh, "A phase-change via-reconfigurable CMOS *LC* VCO," *IEEE Trans. Electron Devices*, vol. 60, no. 12, pp. 3979–3988, Dec. 2013.

[46] A. Zylbersztejn and N. F. Mott, "Metal-insulator transition in vanadium dioxide," *Phys. Rev. B, Condens. Matter*, vol. 11, no. 11, p. 4383, 1975.

[47] D. E. Anagnostou, D. Torres, T. S. Teeslink, and N. Sepulveda, "Vanadium dioxide (VO_2) for reconfigurable antennas and microwave devices: Enabling RF reconfigurability through smart materials," *IEEE Antennas Propag. Mag.*, vol. 62, no. 3, pp. 58–73, Jun. 2020.

[48] F. Dumas-Bouchiat, C. Champeaux, A. Catherinot, A. Crunteanu, and P. Blondy, "RF-microwave switches based on reversible semiconductor-metal transition of VO_2 thin films synthesized by pulsed-laser deposition," *Appl. Phys. Lett.*, vol. 91, no. 22, Nov. 2007, Art. no. 223505.

[49] S. D. Ha, Y. Zhou, C. J. Fisher, S. Ramanathan, and J. P. Treadway, "Electrical switching dynamics and broadband microwave characteristics of VO_2 radio frequency devices," *J. Appl. Phys.*, vol. 113, no. 18, May 2013, Art. no. 184501.

[50] K. Pan, W. Wang, E. Shin, K. Freeman, and G. Subramanyam, "Vanadium oxide thin-film variable resistor-based RF switches," *IEEE Trans. Electron Devices*, vol. 62, no. 9, pp. 2959–2965, Sep. 2015.

[51] J. Jiang, G. Chugunov, and R. R. Mansour, "Fabrication and characterization of VO_2-based series and parallel RF switches," in *IEEE MTT-S Int. Microw. Symp. Dig.*, Jun. 2017, pp. 278–280.

[52] C. Hillman, P. A. Stupar, J. B. Hacker, Z. Griffith, M. Field, and M. Rodwell, "An ultra-low loss millimeter-wave solid state switch technology based on the metal–insulator–transition of vanadium dioxide," in *IEEE MTT-S Int. Microw. Symp. Dig.*, Jun. 2014, pp. 1–4.

[53] J. Givernaud *et al.*, "Microwave power limiting devices based on the semiconductor–metal transition in vanadium–dioxide thin films," *IEEE Trans. Microw. Theory Techn.*, vol. 58, no. 9, pp. 2352–2361, Sep. 2010.

[54] S. Pi, M. Ghadiri-Sadrabadi, J. C. Bardin, and Q. Xia, "Memristors as radiofrequency switches," in *Proc. IEEE Int. Symp. Circuits Syst.*, May 2016, pp. 377–380.

[55] N. Wainstein and S. Kvatinsky, "An RF memristor model and memristive single-pole double-throw switches," in *Proc. IEEE Int. Symp. Circuits Syst. (ISCAS)*, May 2017, pp. 1–4.

[56] N. Wainstein and S. Kvatinsky, "A lumped RF model for nanoscale memristive devices and nonvolatile single-pole double-throw switches," *IEEE Trans. Nanotechnol.*, vol. 17, no. 5, pp. 873–883, Sep. 2018.

[57] G. M. Rebeiz, "RF MEMS switches: Status of the technology," in *Proc. 12th Int. Conf. Solid-State Sensors, Actuat. Microsyst.*, vol. 2, Jun. 2003, pp. 1726–1729.

[58] G. M. Rebeiz *et al.*, "Tuning in to RF MEMS," *IEEE Microw. Mag.*, vol. 10, no. 6, pp. 55–72, Sep. 2009.

[59] H. Wei, Z. Deng, X. Guo, Y. Wang, and H. Yang, "High on/off capacitance ratio RF MEMS capacitive switches," *J. Micromech. Microeng.*, vol. 27, no. 5, Mar. 2017, Art. no. 055002.

[60] S. Gopalakrishnan, A. DasGupta, and D. R. Nair, "Novel RF MEMS capacitive switches with design flexibility for multi-frequency operation," *J. Micromech. Microeng.*, vol. 27, no. 9, Aug. 2017, Art. no. 095013.

[61] M. Li, J. Zhao, Z. You, and G. Zhao, "Design and fabrication of a low insertion loss capacitive RF MEMS switch with novel micro-structures for actuation," *Solid-State Electron.*, vol. 127, pp. 32–37, Jan. 2017.

[62] Analog Devices. (2018). *ADGM1004—0 Hz/DC to 13 GHz, 2.5 kV HBM ESD, SP4T, MEMS Switch With Integrated Driver*. [Online]. Available: https://www.analog.com/en/products/adgm1004.html#product-overview

[63] D. E. Anagnostou *et al.*, "Design, fabrication, and measurements of an RF-MEMS-based self-similar reconfigurable antenna," *IEEE Trans. Antennas Propag.*, vol. 54, no. 2, pp. 422–432, Feb. 2006.

[64] B. A. Cetiner, G. R. Crusats, L. Jofre, and N. Biyikli, "RF MEMS integrated frequency reconfigurable annular slot antenna," *IEEE Trans. Antennas Propag.*, vol. 58, no. 3, pp. 626–632, Mar. 2010.

[65] K. Entesari and G. M. Rebeiz, "A differential 4-bit 6.5–10-GHz RF MEMS tunable filter," *IEEE Trans. Microw. Theory Techn.*, vol. 53, no. 3, pp. 1103–1110, Mar. 2005.

[66] G. R. Bhimanapati *et al.*, "Recent advances in two-dimensional materials beyond graphene," *ACS Nano*, vol. 9, no. 12, pp. 11509–11539, Nov. 2015.

[67] R. Ge *et al.*, "Atomristor: Nonvolatile resistance switching in atomic sheets of transition metal dichalcogenides," *Nano Lett.*, vol. 18, no. 1, pp. 434–441, Dec. 2017.

[68] R. Ge *et al.*, "Atomristors: Memory effect in atomically-thin sheets and record RF switches," *IEDM Tech. Dig.*, Dec. 2018, pp. 532–535.

[69] M. Kim *et al.*, "Non-volatile RF and mm-wave switches based on monolayer hBN," in *IEDM Tech. Dig.*, Feb. 2020, pp. 9.5.1–9.5.4.

[70] I. Valov and G. Staikov, "Nucleation and growth phenomena in nanosized electrochemical systems for resistive switching memories," *J. Solid State Electrochem.*, vol. 17, no. 2, pp. 365–371, Feb. 2013.

[71] S. Yu and H.-S. P. Wong, "Compact modeling of conducting-bridge," *IEEE Trans. Electron Devices*, vol. 58, no. 5, pp. 1352–1360, May 2011.

[72] D. B. Strukov, "Endurance-write-speed tradeoffs in nonvolatile memories," *Appl. Phys. A, Mater. Sci. Process.*, vol. 122, no. 4, pp. 1–4, Mar. 2016.

[73] M. D. Gregory and D. H. Werner, "Application of the memristor in reconfigurable electromagnetic devices," *IEEE Antennas Propag. Mag.*, vol. 57, no. 1, pp. 239–248, Mar. 2015.

[74] R. Badulescu *et al.*, "Novel metal oxide resistive switches for tunable radio frequency circuits," in *Proc. Innov. Sustainability Conf.*, vol. 40, 2017, pp. 1–4.

[75] M.-J. Lee *et al.*, "A fast, high-endurance and scalable non-volatile memory device made from asymmetric Ta_2O_{5-x}/TaO_{2-x} bilayer structures," *Nature Mater.*, vol. 10, no. 8, pp. 625–630, Jul. 2011.

[76] C. W. Hsu *et al.*, "Homogeneous barrier modulation of TaO_x/TiO_2 bilayers for ultra-high endurance three-dimensional storage-class memory," *Nanotechnology*, vol. 25, no. 16, Mar. 2014, Art. no. 165202.

[77] S. K. Kim, K. M. Kim, D. S. Jeong, W. Jeon, K. J. Yoon, and C. S. Hwang, "Titanium dioxide thin films for next-generation memory devices," *J. Mater. Res.*, vol. 28, no. 3, pp. 313–325, Jul. 2013.

[78] Y. Shim, G. Hummel, and M. Rais-Zadeh, "RF switches using phase change materials," in *Proc. IEEE 26th Int. Conf. Micro Electro Mech. Syst. (MEMS)*, Jan. 2013, pp. 237–240.

[79] A. Crunteanu, L. Huitema, J.-C. Orlianges, C. Guines, and D. Passerieux, "Optical switching of GeTe phase change materials for high-frequency applications," in *IEEE MTT-S Int. Microw. Symp. Dig.*, Sep. 2017, pp. 1–3.

[80] A. Ghalem, C. Guines, D. Passerieux, J.-C. Orlianges, L. Huitema, and A. Crunteanu, "Reversible, fast optical switching of phase change materials for active control of high-frequency functions," in *IEEE MTT-S Int. Microw. Symp. Dig.*, Jun. 2018, pp. 839–842.

[81] R. Wolf, A. Joseph, A. Botula, and J. Slinkman, "A thin-film SOI 180 nm CMOS RF switch," in *Proc. IEEE Topical Meeting Silicon Monolithic Integr. Circuits RF Syst.*, Jan. 2009, pp. 1–4.

[82] A. Léon, B. Reig, V. Puyal, E. Perret, P. Ferrari, and F. Podevin, "High performance and low energy consumption in phase change material RF switches," in *Proc. 48th Eur. Microw. Conf. (EuMC)*, Nov. 2018, pp. 491–494.

[83] C.-Y. Wen *et al.*, "A phase-change via-reconfigurable on-chip inductor," in *IEDM Tech. Dig.*, Dec. 2010, pp. 237–240.

[84] N. El-Hinnawy *et al.*, "Reconfigurable inline phase-change switches for broadband applications," in *IEEE MTT-S Int. Microw. Symp. Dig.*, May 2015, pp. 1–4.

[85] M. Wang and M. Rais-Zadeh, "Directly heated four-terminal phase change switches," in *IEEE MTT-S Int. Microw. Symp. Dig.*, Jun. 2014, pp. 1–4.

[86] G. Slovin, M. Xu, R. Singh, T. E. Schlesinger, J. Paramesh, and J. A. Bain, "Design criteria in

sizing phase-change RF switches," *IEEE Trans. Microw. Theory Techn.*, vol. 65, no. 11, pp. 4531–4540, Nov. 2017.
[87] N. El-Hinnawy *et al.*, "12.5 THz Fco GeTe inline phase-change switch technology for reconfigurable RF and switching applications," in *Proc. IEEE Compound Semiconductor Integr. Circuit Symp. (CSICS)*, Oct. 2014, pp. 14–16.
[88] R. M. O. Young *et al.*, "Improvements in GeTe-based phase change RF switches," in *IEEE MTT-S Int. Microw. Symp. Dig.*, Jun. 2018, pp. 832–835.
[89] J.-S. Moon, H.-C. Seo, K.-A. Son, K. Lee, D. Zehnder, and H. Tai, "5 THz figure-of-merit reliable phase-change RF switches for millimeter-wave applications," in *IEEE MTT-S Int. Microw. Symp. Dig.*, Jun. 2018, pp. 1–3.
[90] E. Yalon, I. M. Datye, J.-S. Moon, K.-A. Son, K. Lee, and E. Pop, "Energy-efficient indirectly heated phase change RF switch," *IEEE Electron Device Lett.*, vol. 40, no. 3, pp. 455–458, Mar. 2019.
[91] J.-S. Moon, H.-c. Seo, and D. Le, "Development toward high-power sub-1-Ohm DC-67 GHz RF switches using phase change materials for reconfigurable RF front-end," in *IEEE MTT-S Int. Microw. Symp. Dig.*, Jun. 2014, pp. 1–3.
[92] N. El-Hinnawy *et al.*, "A 7.3 THz cut-off frequency, inline, chalcogenide phase-change RF switch using an independent resistive heater for thermal actuation," in *Proc. IEEE Compound Semiconductor Integr. Circuit Symp. (CSICS)*, Oct. 2013, pp. 1–4.
[93] N. El-Hinnawy *et al.*, "Experimental demonstration of AlN heat spreaders for the monolithic integration of inline phase-change switches," *IEEE Electron Device Lett.*, vol. 39, no. 4, pp. 610–613, Apr. 2018.
[94] P. Hurwitz, R. Kanawati, K. Moen, E. Preisler, S. Chaudhry, and M. Racanelli, "Advances in RF foundry technology for wireless and wireline communications," in *Proc. IEEE 16th Top. Meeting Silicon Monolithic Integr. Circuits RF Syst. (SiRF)*, Jan. 2016, pp. 5–8.
[95] R. Stefanini, M. Chatras, P. Blondy, and G. M. Rebeiz, "Miniature MEMS switches for RF applications," *J. Microelectromech. Syst.*, vol. 20, no. 6, pp. 1324–1335, Dec. 2011.
[96] A. Scavennec, M. Sokolich, and Y. Baeyens, "Semiconductor technologies for higher frequencies," *IEEE Microw. Mag.*, vol. 10, no. 2, pp. 77–87, Apr. 2009.
[97] H. Kamitsuna, Y. Yamane, M. Tokumitsu, H. Sugahara, and M. Muraguchi, "Low-power InP-HEMT switch ICs integrating miniaturized 2×2 switches for 10-Gb/s systems," *IEEE J. Solid-State Circuits*, vol. 41, no. 2, pp. 452–460, Feb. 2006.
[98] M. Uzunkol and G. M. Rebeiz, "140–220 GHz SPST and SPDT switches in 45 nm CMOS SOI," *IEEE Microw. Wireless Compon. Lett.*, vol. 22, no. 8, pp. 412–414, Aug. 2012.
[99] M. Jaffe *et al.*, "Improvements in SOI technology for RF switches," in *Proc. IEEE 15th Top. Meeting Silicon Monolithic Integr. Circuits RF Syst.*, Jan. 2015, pp. 30–32.
[100] M. D. Yore, C. A. Nevers, and P. Córtese, "High-isolation low-loss SP7T pHEMT switch suitable for antenna switch modules," in *Proc. Eur. Microw. Integr. Circuits Conf. (EuMIC)*, Sep. 2010, pp. 69–72.
[101] R. S. Howell *et al.*, "Low loss, high performance 1–18 GHz SPDT based on the novel super-lattice castellated field effect transistor (SLCFET)," in *Proc. IEEE Compound Semiconductor Integr. Circuit Symp. (CSICS)*, Oct. 2014, pp. 1–5.
[102] T. Boles, J. Brogle, D. Hoag, and D. Curcio, "AlGaAs PIN diode multi-octave, mmW switches," in *Proc. IEEE Int. Conf. Microw., Commun., Antennas Electron. Syst. (COMCAS)*, Nov. 2011, pp. 1–5.
[103] M. Li, J. Zhao, Z. You, and G. Zhao, "Design and fabrication of a low insertion loss capacitive RF MEMS switch with novel micro-structures for actuation," *Solid-State Electron.*, vol. 127, pp. 32–37, Jan. 2017.
[104] P. Borodulin *et al.*, "Recent advances in fabrication and characterization of GeTe-based phase-change RF switches and MMICs," in *IEEE MTT-S Int. Microw. Symp. Dig.*, Oct. 2017, pp. 285–288.
[105] A. Hariri, A. Crunteanu, C. Guines, C. Hallepee, D. Passerieux, and P. Blondy, "Double-port double-throw (DPDT) switch matrix based on phase change material (PCM)," in *Proc. 48th Eur. Microw. Conf. (EuMC)*, Sep. 2018, pp. 479–482.
[106] N. El-Hinnawy *et al.*, "Substrate agnostic monolithic integration of the inline phase-change switch technology," in *IEEE MTT-S Int. Microw. Symp. Dig.*, Aug. 2016, pp. 1–4.
[107] T. Singh and R. R. Mansour, "Miniaturized DC–60 GHz RF PCM GeTe-based monolithically integrated redundancy switch matrix using T-type switching unit cells," *IEEE Trans. Microw. Theory Techn.*, vol. 67, no. 12, pp. 5181–5190, Dec. 2019.
[108] N. Wainstein and S. Kvatinsky, "TIME—Tunable inductors using MEmristors," *IEEE Trans. Circuits Syst. I, Reg. Papers*, vol. 65, no. 5, pp. 1505–1515, May 2018.
[109] L. Chau *et al.*, "Reconfigurable antenna aperture with optically controlled GeTe-based RF switches," Northrop Grumman Aerosp. Syst., Redondo Beach, CA, USA, Tech. Rep. NGAS 14-3165, 2015.
[110] H. Wong, Q.-Y. Guo, A. Crunteanu, and L. Huitema, "A 30 GHz pattern reconfigurable antenna using phase-change material," in *Proc. Int. Conf. Microw. Millim. Wave Technol. (ICMMT)*, Feb. 2019, pp. 1–3.
[111] M. Wang, F. Lin, and M. Rais-Zadeh, "Need a change? Try GeTe: A reconfigurable filter using germanium telluride phase change RF switches," *IEEE Microw. Mag.*, vol. 17, no. 12, pp. 70–79, Dec. 2016.
[112] B. Razavi, "Architectures and circuits for RF CMOS receivers," in *Proc. IEEE Custom Integr. Circuits Conf.*, May 1998, pp. 393–400.
[113] R. Singh, G. Slovin, M. Xu, T. E. Schlesinger, J. A. Bain, and J. Paramesh, "A reconfigurable dual-frequency narrowband CMOS LNA using phase-change RF switches," *IEEE Trans. Microw. Theory Techn.*, vol. 65, no. 11, pp. 4689–4703, Nov. 2017.
[114] N. Wainstein, T. Tsabari, Y. Goldin, E. Yalon, and S. Kvatinsky, "A dual-band CMOS low-noise amplifier using memristor-based tunable inductors," in *Proc. IEEE Comput. Soc. Annu. Symp. VLSI*, Jul. 2019, pp. 1–6.
[115] B. Razavi, *RF Microelectronics*. Upper Saddle River, NJ, USA: Prentice-Hall, 2012.
[116] D. Ham and A. Hajimiri, "Concepts and methods in optimization of integrated LC VCOs," *IEEE J. Solid-State Circuits*, vol. 36, no. 6, pp. 896–909, Jun. 2001.
[117] T.-Y. Lu, C.-Y. Yu, W.-Z. Chen, and C.-Y. Wu, "Wide tunning range 60 GHz VCO and 40 GHz DCO using single variable inductor," *IEEE Trans. Circuits Syst. I, Reg. Papers*, vol. 60, no. 2, pp. 257–267, Feb. 2013.

ABOUT THE AUTHORS

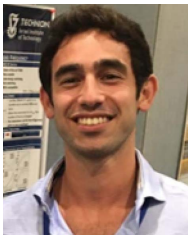

Nicolás Wainstein (Graduate Student Member, IEEE) received the degree in electrical engineering from the Universidad de la República, Montevideo, Uruguay, in 2014. He is working toward the Ph.D. degree at the Andrew and Erna Viterbi Faculty of Electrical Engineering, Technion–Israel Institute of Technology, Haifa, Israel.

His current research interests include radio frequency and analog circuits and systems based on resistive memory technologies.

Mr. Wainstein was a recipient of the 2020 Yablonovitch Research Prize, the 2020 RBNI Prize for Excellence in Nanoscience and Nanotechnology, the 2020 RBNI Scholarship, the 2019 Jury Award for Outstanding Students, and the Excellence Scholarship from the Andrew and Erna Viterbi Faculty of Electrical Engineering, Technion—Israel Institute of Technology, in 2018, 2019, and 2020.

Gina Adam (Member, IEEE) received the B.Sc. degree in applied electronics from the University Politehnica of Bucharest, Bucharest, Romania, in 2010, and the Ph.D. degree in electrical and computer engineering from the University of California at Santa Barbara, Santa Barbara, CA, USA, in 2015.

From 2016 to 2018, she was a Research Scientist with the National Institute for Research and Development in Microtechnologies, Voluntari, Romania, and a Visiting Scholar with the École Polytechnique Fédérale de Lausanne, Lausanne, Switzerland. She is currently an Assistant Professor of electrical and computer engineering with the School of Engineering and Applied Science, George Washington University, Washington, DC, USA. Her current research interests include resistive switching devices and their use in memory storage, computing, and communications applications.

Dr. Adam was a recipient of the International Fulbright Science and Technology Award in 2010, the Mirzayan Fellowship at the National Academy of Engineering in 2012, and the H2020 Marie Sklodowska-Curie Grant from the European Commission in 2016 and 2018.

Eilam Yalon (Member, IEEE) received the B.Sc. degree in materials engineering and physics and the Ph.D. degree in electrical engineering from the Technion—Israel Institute of Technology, Haifa, Israel, in 2009 and 2015, respectively.

From 2015 to 2018, he was a Postdoctoral Researcher with Stanford University, Stanford, CA, USA. He is currently an Assistant Professor with the Andrew and Erna Viterbi Faculty of Electrical Engineering, Technion—Israel Institute of Technology. His current research interests include energy-efficient memory and computing devices with 2-D materials, resistive switching oxides, and phase-change chalcogenides.

Shahar Kvatinsky (Senior Member, IEEE) received the B.Sc. degree in computer engineering and applied physics and the M.B.A. degree from The Hebrew University of Jerusalem, Jerusalem, Israel, in 2009 and 2010, respectively, and the Ph.D. degree in electrical engineering from the Technion–Israel Institute of Technology, Haifa, Israel, in 2014.

From 2006 to 2009, he worked as a Circuit Designer at Intel, Jerusalem. From 2014 to 2015, he was a Postdoctoral Research Fellow with Stanford University, Stanford, CA, USA. He is currently an Associate Professor with the Andrew and Erna Viterbi Faculty of Electrical Engineering, Technion–Israel Institute of Technology. His current research interests include circuits and architectures with emerging memory technologies and design of energy efficient architectures.

Dr. Kvatinsky was a recipient of numerous awards, including the 2020 MDPI Electronics Young Investigator Award, the 2019 Wolf Foundation's Krill Prize for Excellence in Scientific Research, the 2015 IEEE Guillemin-Cauer Best Paper Award, the 2015 Best Paper of Computer Architecture Letters, the Viterbi Fellowship, the Jacobs Fellowship, the ERC Starting Grant, the 2017 Pazy Memorial Award, the 2014 and 2017 Hershel Rich Technion Innovation Awards, the 2013 Sanford Kaplan Prize for Creative Management in High Tech, the 2010 Benin prize, and the Seven Technion Excellence Teaching Awards. He is an Editor of *Microelectronics Journal*.